Supporting information for:

The kinetics and mechanism of the interconversion within a system of $[Fe_2L_3]^{4+}$ helicates and $[Fe_4L_6]^{8+}$ cages

Rashid G. Siddique,[a] Kasun S. A. Arachchige,[a] Hydar A. AL-Fayaad,[a] Aidan J. Brock,[b] Aaron S. Micallef,[b] Ena T. Luis,[b] John D. Thoburn,[c] John C. McMurtrie[b] and Jack K. Clegg*[a]

[a] School of Chemistry and Molecular Biosciences, The University of Queensland, St. Lucia, Queensland, 4072, Australia. j.clegg@uq.edu.au

[b]School of Chemistry and Physics and Centre for Materials Science, Queensland University of Technology (QUT), Brisbane, Queensland 4000, Australia

[c]Department of Chemistry, Randolph-Macon College, Ashland, VA 23005, USA

Table of Contents

1 Experimental

1.1 General

All reagents were purchased from different commercial sources like Merck, sigma Aldrich and VWR and used without further purification. $[PdCl_2(PPh_3)_2]$, $[Pd(PPh_3)_4]$ and $[Cu(CH_3CN)_4]PF_6$ were synthesised using established methodologies.[1, 2] The solvents were dried using Innovative Technologies Pure Solv solvent purification system. Silica gel (mesh size 230-400) was used as stationary phase for flash chromatography, and the precoated silica 60 gel plate was used for TLC and UV lamp was mainly used as detection source. For Suzuki couplings, the solvents were degassed using vacuum-N2 bicycle on Schlenk line. NMR spectra were recorded on Bruker Avance 300 MHz, Bruker ASCEND 500 MHz spectrometer and Bruker AVANCE 500 MHz spectrometer were used to record ^{1}H, 2D COSY, 2D DOSY and ^{13}C NMR spectra. All DOSY experiments were performed on Bruker AVANCE 500 MHz spectrometer using standard Bruker program, ledbpg2s. A stimulated echo and longitudinal eddy-current delay (LED) was employed using bipolar gradient pulses for diffusion. In a typical DOSY experiment, the gradient pulse duration was varied between 2 and 2.4 ms, the diffusion time was 20 ms, a series of 16 spectra on 32K data points were recorded and the pulse gradients were incremented from 5 to 95%. The data was processed using Bruker Topspin 3.6 and MestReNova v. 12 and the Stokes-Einstein equation was employed to calculate the hydrodynamic radius from the resulting diffusion coefficient. In-situ NMR spectra for kinetics study were recorded on either Bruker Avance III 400 MHz spectrometer, equipped with a 5mm BBO probe with z-gradients or Bruker ASCEND 500 MHz spectrometer. Mass spectrometry was performed on Bruker MicroTOFQ, Bruker HCT and Thermo LCQ Fleet mass spectrometers using stated solvent. Electrospray ionization mass spectra (ESI-MS) were obtained on a Mass spectrometry was performed on Bruker MicroTOFQ, Bruker HCT and Thermo LCQ Fleet mass spectrometers using stated solvent.

*1.1.1 Synthesis of 2-(tributylstannyl)pyridine (**1**)*

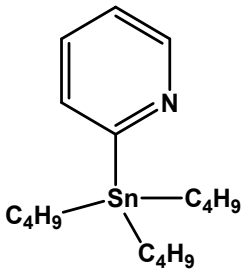

To a solution of 2-bromopyridine (8.5 g, 53.8 mmol) in dry diethyl ether was added n-BuLi (42 mL, 67.2 mmol, 1.6M in hexane) dropwise at -78 °C and the resulting mixture stirred for 2 hours. Tributyl tin chloride (18.2 mL, 67.2 mmol) was added to the reaction mixture and stirring continued at -78 °C for 3 hours and then at room temperature for 12 hours. The mixture was then passed through the plug of celite and the solvent is evaporated under reduced pressure. The resulting crude product (yield 97%) was used as such in the next step without any further purification. The ^{1}H NMR was consistent with that previously reported.[3]

*1.1.2 Synthesis of 5-bromo-2,2'-bipyridine (**2**)*

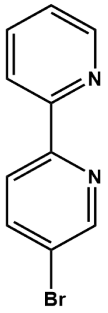

Crude 2-(tributylstannyl)pyridine (8.41 g, 22.90 mmol) and 2, 5-dibromopyridine (6.77 g, 28.60 mmol) were added into a 2-necked round bottom flask. The atmosphere was purged with argon and dry toluene (150 mL) was then transferred via syringe. The mixture was degassed three times using vacuum-argon bicycle on Schlenk line. After adding [$Pd(PPh_3)_4$] (800 mg ,0.69 mmol), the reaction mixture was refluxed for 3 d under argon. The mixture was cooled in an ice bath and approximately 100 mL of 1M NaOH added. The layers were separated and the aqueous layer was re-extracted with toluene 3 x 100 mL. The combined organic layers were washed with H_2O, brine, dried over $MgSO_4$ and filtered before evaporating the solvent in vacuo. The crude product was then purified by column chromatography using 85:15 petroleum spirits: ethyl acetate. The silica was first neutralized with 85:15:2 petroleum spirits: ethyl acetate: triethylamine and subsequently rinsed with 85:15 petroleum spirits: ethyl acetate in the column before the sample was dry loaded on silica (3.6 g, 67%). ^{1}H NMR (300 MHz, $CDCl_3$,

δ/ppm, J/Hz) 7.36-7.30 (ddd, 1H, 6.0, 4.8, 1.2 Hz), 7.85-7.78 (ddd, 1H, 8.0, 7.5, 1.8 Hz), 7.96-7.91 (dd, 1H, 8.5, 2.4 Hz), 8.34-8.29 (dd, 1H, 8.5, 0.7 Hz), 8.39-8.35 (td, 1H, 8.0, 1.1 Hz) 8.69-8.64 (ddd, 1H, 4.0, 1.8, 0.9), 8.73-8.70 (dd, 1H, 2.4, 0.7 Hz). The ^{1}H NMR was matched with previously reported procedure.[3]

*1.1.3 Synthesis of 1,4-dibromo-2,5-diiodobenzene (**3**)*

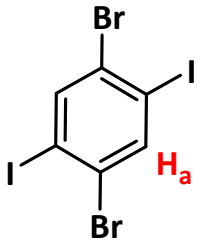

1,4 dibromo benzene (31 g, 131.4 mmol) was dissolved in of conc. H_2SO_4 (500 mL) at 60 °C, and Iodine (73 g, 575.25 mmol) was added slowly in five portions over 2 hours. The reaction mixture was vigorously stirred while it was held at 130 °C for 2 d. The mixture was cooled at room temperature and poured into ice before extraction into DCM. The DCM layer was washed with dilute NaOH, brine and dried over $MgSO_4$, and the solvent was evaporated under reduced pressure. Large portion of product was in solid form that was crushed, stirred with dilute NaOH and then filtered. The combined products were recrystallized form toluene (47 g, 73 %). ^{1}H NMR (300 MHz, $CDCl_3$, δ/ppm) 8.05 (s, 2H, H_a); ^{13}C NMR (75 MHz, $CDCl_3$, δ/ppm): 101.3, 129.2, 142.3. Both ^{1}H NMR and ^{13}C NMR were matched with those of previously reported procedure.[4]

*1.1.4 Synthesis of (2,5-dibromo-1,4-phenylene)bis(ethyne-2,1-diyl))bis(trimethylsilane) (**4**)*

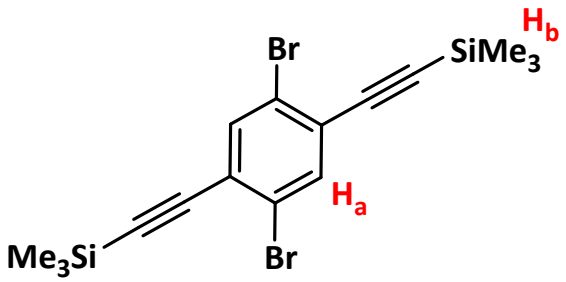

Compound **3** (45 g, 92.26 mmol) was dissolved in toluene (300 mL) and dry triethylamine (100 mL) and the mixture was purged with N_2 for an hour. Then CuI (0.87g, 4.56 mmol) and $[PdCl_2(PPh_3)_2]$ (1.83 g, 2.61 mmol) were added before dropwise addition of trimethylsilylacetylene (19.03g, 193.74 mmol, 2.1 equivalent) and the reaction mixture was stirred for three days at room temperature under N_2 atmosphere. The reaction was quenched

with water and solvents were evaporated under reduced pressure. After removal of solvent, the product was mixed with 300 mL of petroleum ether and passed through plug of silica gel. The filtrate is concentrated under reduced pressure and the resulting product was thoroughly washed with cold methanol to form off white precipitates (34 g, 86 %). ^{1}H NMR (300 MHz, $CDCl_3$, δ/ppm): 7.67 (s, 2H, H_a), 0.27 (s, 18H, H_b). ^{13}C NMR (75 MHz, $CDCl_3$, δ/ppm): -0.4, 101.3, 103.5, 123.6, 126.4, 136.4. Both ^{1}H NMR and ^{13}C NMR spectra were consistent with the previous report.[5]

*1.1.5 Synthesis of ((2,5-bis(4,4,5,5-tetramethyl-1,3,2-dioxaborolan-2-yl) -1,4-phenylene) bis(ethyne-2,1-diyl))bis(trimethylsilane) (**5**)*

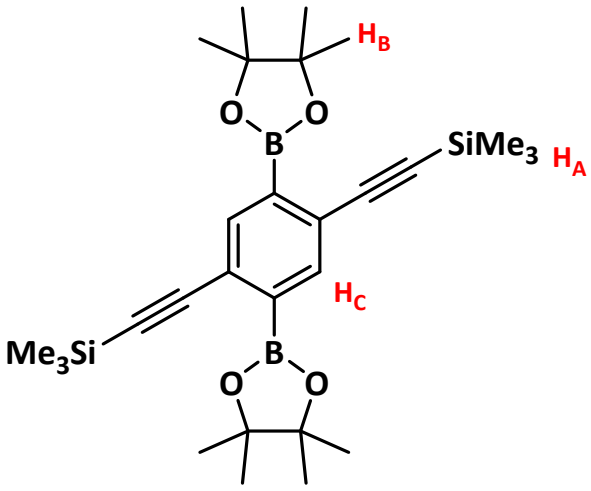

Compound **5** was synthesised by reacting **4** (30 g, 70.04 mmol) with bis(pinacolato)diboron (37.35g, 147.08 mmol, 2.1 equivalent) in N2-purged 1,4-dioxane (400 mL) in the presence of potassium acetate (20.62 g, 210.12 mmol, 3 equivalent) and $[PdCl_2(PPh_3)_2]$ (3g, 4.3 mmol). The reaction mixture was refluxed for 3d under N2 atmosphere. The 1,4-dioxane was removed under reduced pressure and the product was dissolved in 1: 10 mixture of ethyl acetate and petroleum ether and passed through a plug of silica gel. The resulting filtrate was evaporated and the product was thoroughly washed with petroleum ether and then acetone and used for the next step without any further purification (28 g, 76 %). ^{1}H NMR (300 MHz, $CDCl_3$, δ/ppm) 0.25(s, 18H, H_A), 1.36 (s, 24H, H_B), 7.82 (s, 2H, H_C). ^{13}C NMR (75 MHz, $CDCl_3$, δ/ppm): -0.1, 24.9, 84.4, 97.6, 105.1, 126.6, 139.3. EI-MS; Calculated $(L+H)^+$ m/z = 523.31, found $(L+H)^+$ m/z = 523.3. Elemental analysis: calculated for ($C_{28}H_{44}B_2O_4Si_2$) C = 64.37, H = 8.49; found C =64.20, H = 8.50.

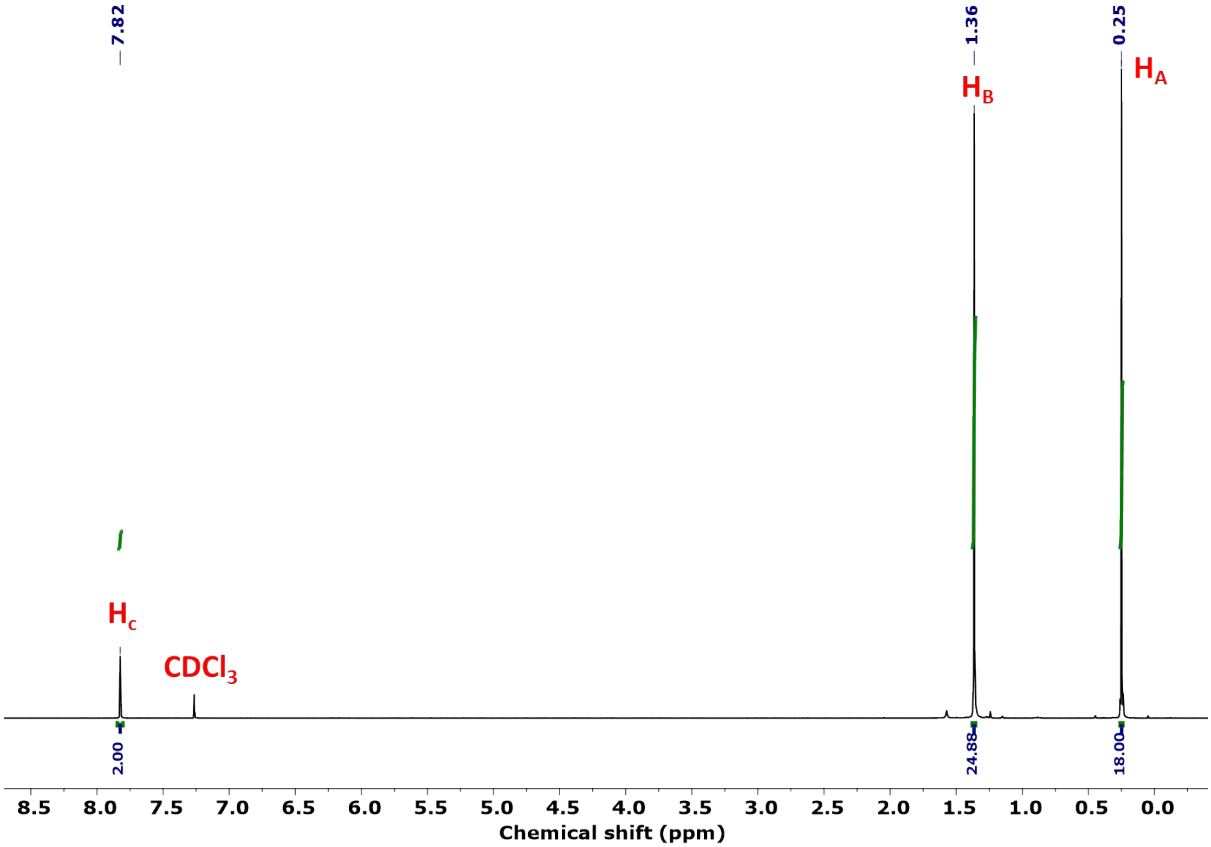

Figure S1. ^{1}H NMR spectrum (300 MHz, $CDCl_3$, 298K) of **5** with peak assignments.

*1.1.6 Synthesis of 5,5''-(2,5-bis((trimethylsilyl)ethynyl)-1,4-phenylene)di-2,2'-bipyridine (**6**)*

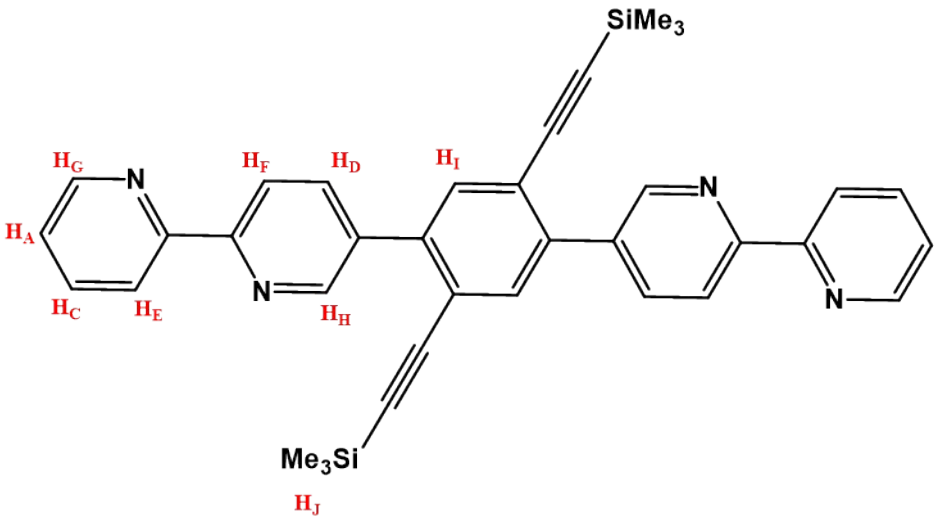

Compound **5** (2 g, 3.83 mmol), preheated K_2CO_3 (4 g, 29 mmol) and 5-bromo-2,2-bipyridine (1.8 g, 7.65 mmol) were dissolved in toluene (80 mL) and water (20 mL) mixture and degassed using vacuum-N_2 bicycle on Schlenk line. After adding $[Pd(PPh_3)_4]$ (500 mg, 0.43 mmol), the reaction mixture was refluxed for 2 d at 100 °C under N_2. After removal of the organic phase

under reduce pressure, the product was extracted into DCM and organic layer was washed with water, brine and dried over anhydrous $MgSO_4$. The DCM layer was concentrated under reduced pressure and the excess methanol was added, the white precipitates were formed after cooling the mixture. The precipitate was thoroughly washed with cold methanol (1.6 g, 72%). 2D COSY and 1D NOESY proton NMR were carried out to assign peaks.^{1}H NMR (500 MHz, $CDCl_3$, δ/ppm, J/Hz): 8.94-8.92 (dd, $2H_H$, 2.2, 0.7 Hz), 8.73-8.70 (ddd, $2H_G$, 4.8, 1.8, 0.9 Hz), 8.49-8.48 (m, $2H_F$), 8.48-8.46 (m, $2H_E$), 8.120-8.11 (dd, $2H_D$, 8.2, 2.4 Hz), 7.88-7.82 (td, $2H_C$, 7.8, 1.8 Hz), 7.70 (s, $2H_I$), 7.36-7.31 (ddd, $2H_A$, 6.2, 4.8, 1.2 Hz), 0.17 (s, $18H_J$). ^{13}C NMR (125 MHz, $CDCl_3$, δ/ppm): -0.6, 101.3, 103.4, 119.8, 121.2, 122.3, 123.7, 134.1, 134.6, 136.9, 137.3, 139.6, 149.2, 149.3, 152.1, 155.9. EI-MS; Calculated $(L+H)^+$ m/z = 579.24, found $(L+H)^+$ m/z = 579.3. Elemental analysis: calculated for ($C_{36}H_{34}N_4Si_2$) C = 74.71, H = 5.92, N= 9.68; found C =74.33, H = 5.90, N= 9.50.

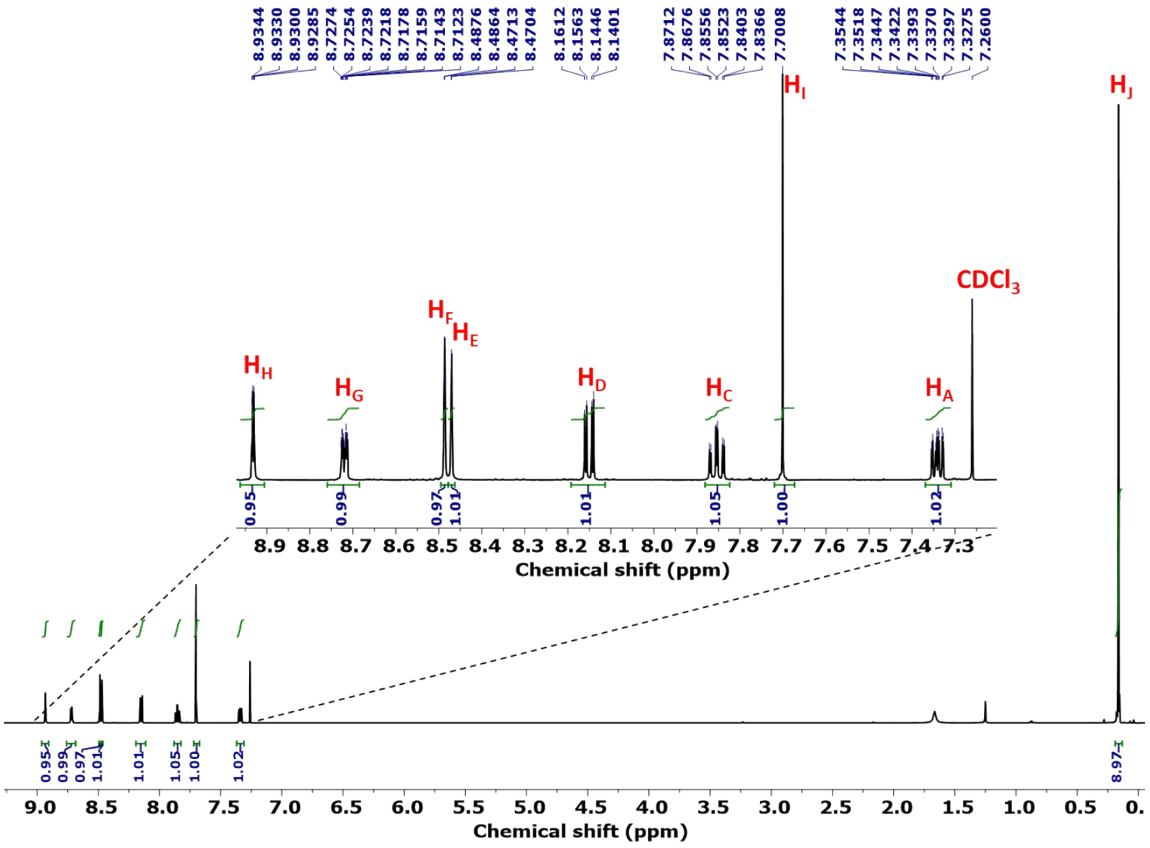

Figure S2. ^{1}H NMR spectrum (500 MHz, $CDCl_3$, 298K) of **6** with peak assignments.

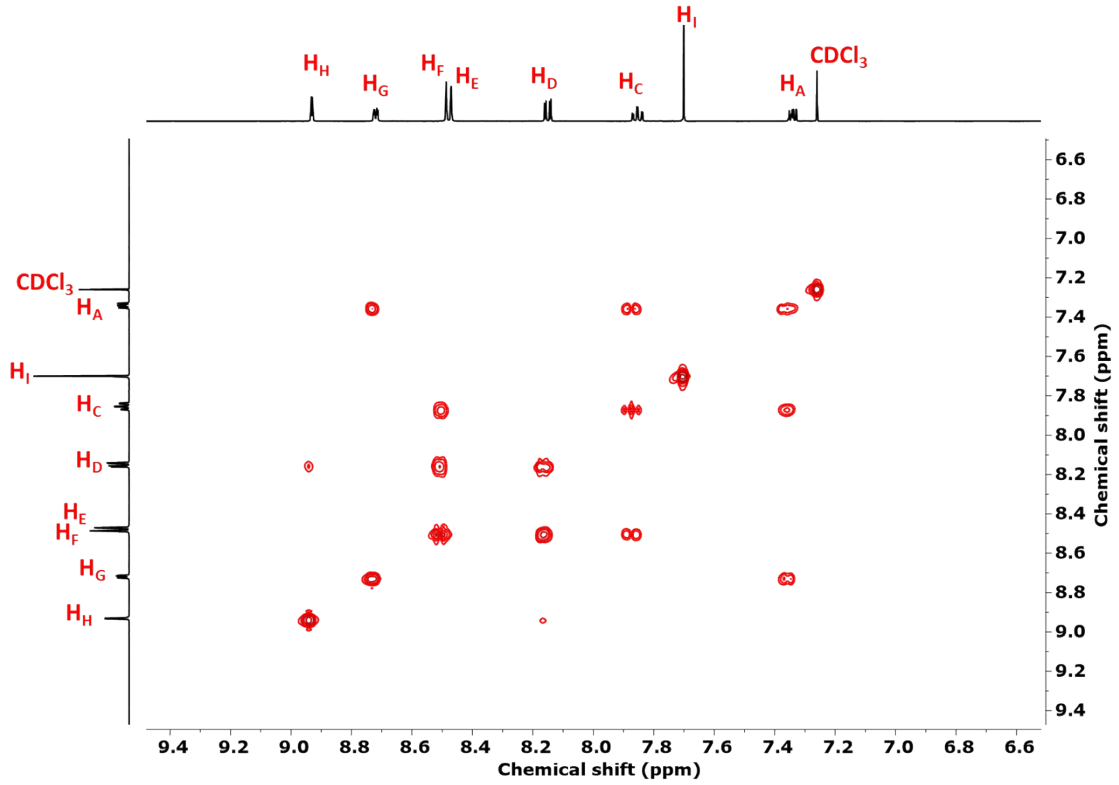

Figure S3. ^{1}H-^{1}H COSY spectrum ($CDCl_3$, 500 MHz, 298K) of **6** in the aromatic region.

*1.1.7 Synthesis of 5,5''-(2,5-diethynyl-1,4-phenylene)di-2,2'-bipyridine (**L**)*

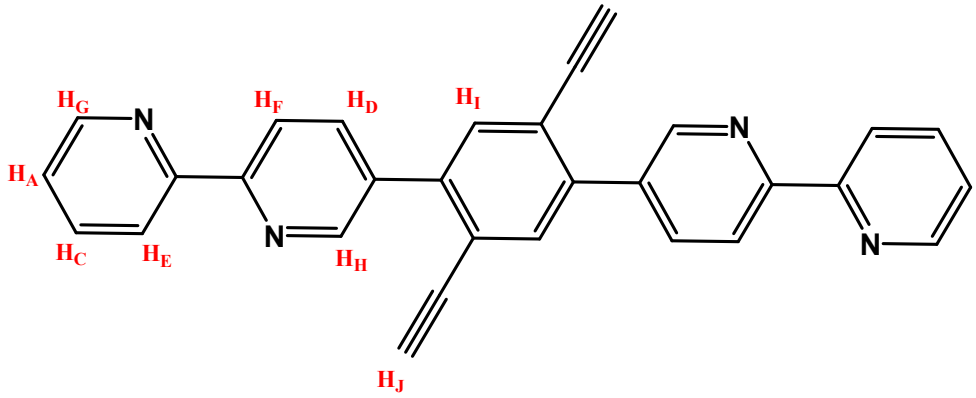

Compound **6** (1.4 g, 2.41 mmol) was added into THF (30 mL), MeOH (30 mL) and 10 % KOH (10 mL) and stirred the resulting mixture at room temperature for 12 hours. The organic solvents were evaporated and diluted the mixture with water and filtered. The precipitates were washed with water and dissolved in the hot chloroform and passed through plug of silica (neutralized with 1% triethylamine), (0.82 g, 78%). ^{1}H NMR (500 MHz, $CDCl_3$, δ/ppm, J/Hz): 8.97-8.94 (dd, $2H_H$, 2.2, 0.7 Hz), 8.77-8.69 (m, $2H_G$), 8.56-8.50 (d, $2H_F$, 8.2 Hz), 8.50-8.44 (d, $2H_E$, 7.9 Hz), 8.15-8.08 (dd, $2H_D$, 8.2, 2.3 Hz), 7.90-7.83(td, $2H_C$, 7.7, 1.6 Hz), 7.75 (s, $2H_I$), 7.39-7.31 (ddd, $2H_A$, 6.3, 4.9, 0.9 Hz), 3.24 (s, $2H_J$). ESI-MS; Calculated $(L+H)^+$ m/z =

435.16096; found $(L+H)^+$ m/z = 435.32. Elemental analysis: calculated for $(C_{30}H_{18}N_4)$ (H_2O), C = 79.61, H = 4.45, N= 12.38; found C =79.95, H = 4.03, N= 12.37.

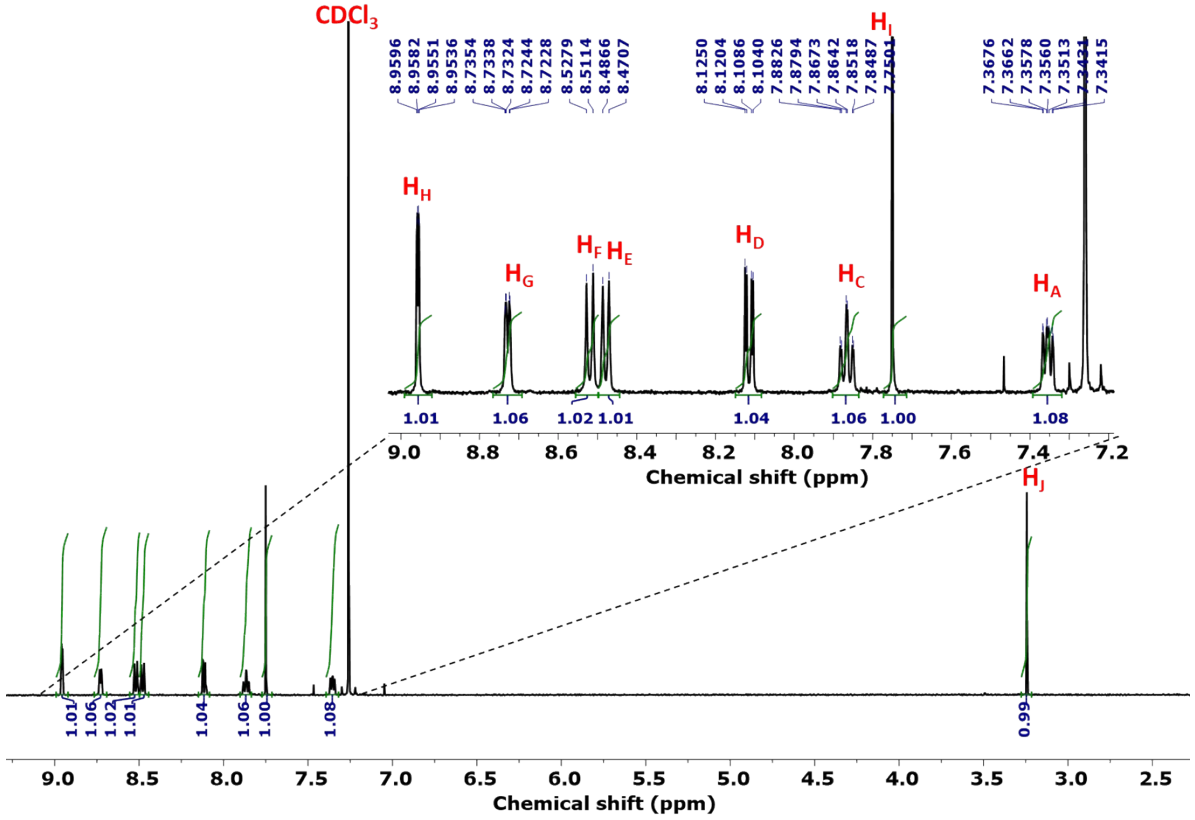

Figure S4. ^{1}H NMR spectrum (500 MHz, $CDCl_3$, 298K) of ligand **L** with peak assignments.

*1.1.8 Synthesis of 1,4-di([2,2'-bipyridin]-5-yl) benzene (**L'**)*

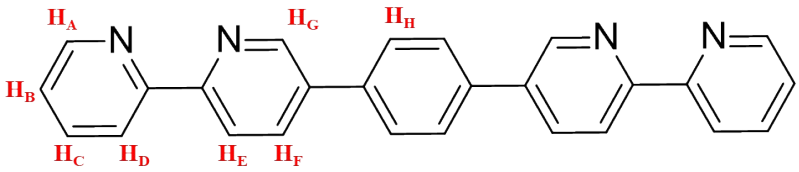

1,4-phenylenediboronic acid (0.4 g, 2.42 mmol), preheated K_2CO_3 (1 g, 7.2 mmol) and 5-bromo-2,2-bipyridine (1.2 g, 5.1 mmol) were added in a mixture of THF (30 mL), water (14 mL) and ethanol (22 mL) and degassed the resulting mixture using vacuum-N_2 bicycle on Schlenk line. After adding [$Pd(PPh_3)_4$] (300 mg, 0.26 mmol), the reaction mixture was refluxed for 2 d at 80 °C under N_2. After removal of the organic phase under reduce pressure, the product was extracted into DCM. The DCM layer was removed under reduced pressure and the product was dry loaded on short plug of silica and first eluted the impurities with DCM and then pure product was obtained by elution of 2:98 mixture of triethylamine and DCM. The filtrate was evaporated under reduced pressure followed by washing with minimum amount of cold methanol afforded pure colourless product (0.8 g, 86%).^{1}H NMR (500 MHz, $CDCl_3$, δ/ppm, J/Hz): 7.35-7.32 (ddd, $2H_B$, 6.1, 4.8, 1.2 Hz), 7.81 (s, $4H_H$), 7.87-7.83 (m, $2H_C$), 8.10-8.08 (dd, $2H_F$, 8.2, 2.4 Hz), 8.48-8.45 (dt, $2H_D$, 7.9, 1.0 Hz), 8.53-8.50 (dd, $2H_E$, 8.4, 0.7 Hz), 8.73-8.70 (ddd, $2H_A$, 4.8, 1.8, 0.8 Hz), 9.0-8.98 (dd, $2H_G$, 2.4, 0.7 Hz). The ^{1}H NMR spectrum matched the previously reported compound.[6]

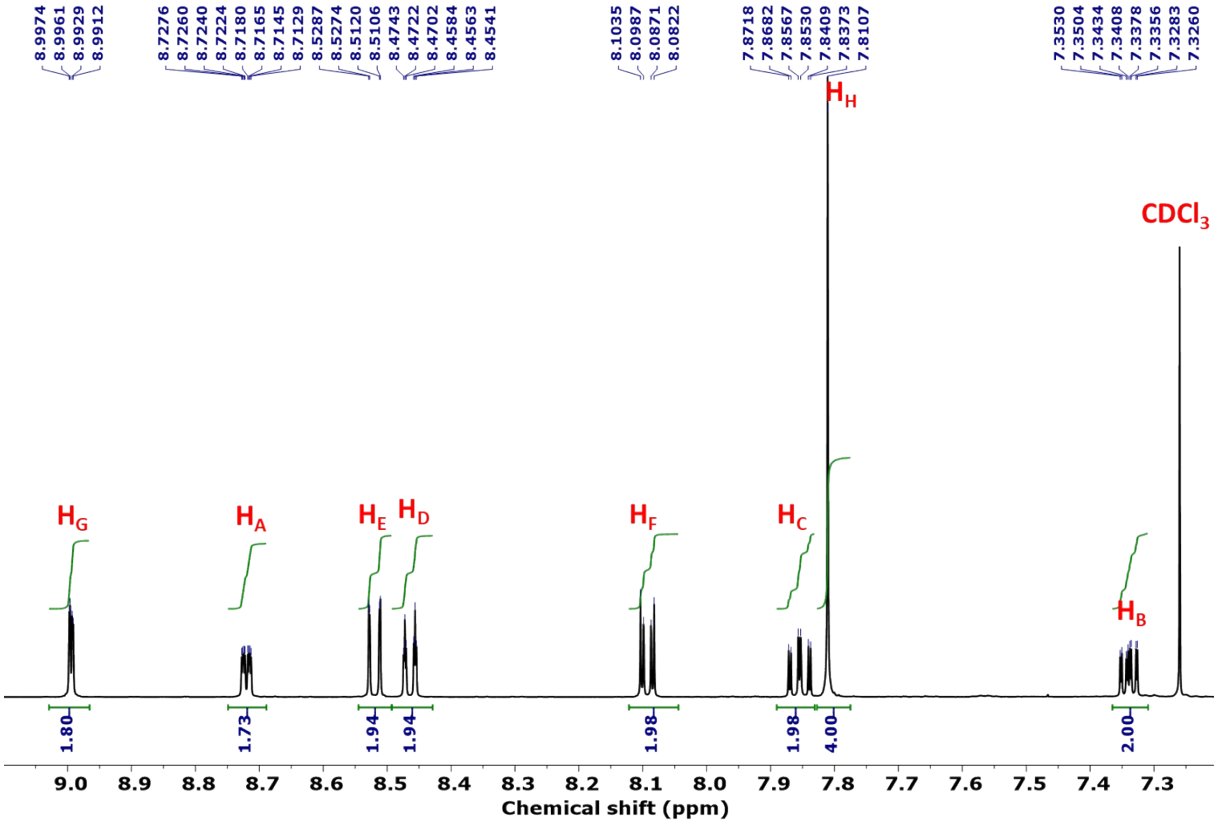

Figure S5. ^{1}H NMR spectrum (500 MHz, $CDCl_3$, 298K) of **L′** with peak assignments.

1.1.9 Synthesis of a mixture of $[Fe_2\mathbf{L}_3]\cdot 4BF_4$ and $[Fe_4\mathbf{L}_6]\cdot 8BF_4$

The ligand **L** (92 mg, 0.21mmol) and $Fe(BF_4)_2\cdot 6H_2O$ (48mg, 0.14 mmol) were mixed into acetonitrile (22 mL) and the reaction mixture was heated in microwave for 30 minutes at 130 °C.

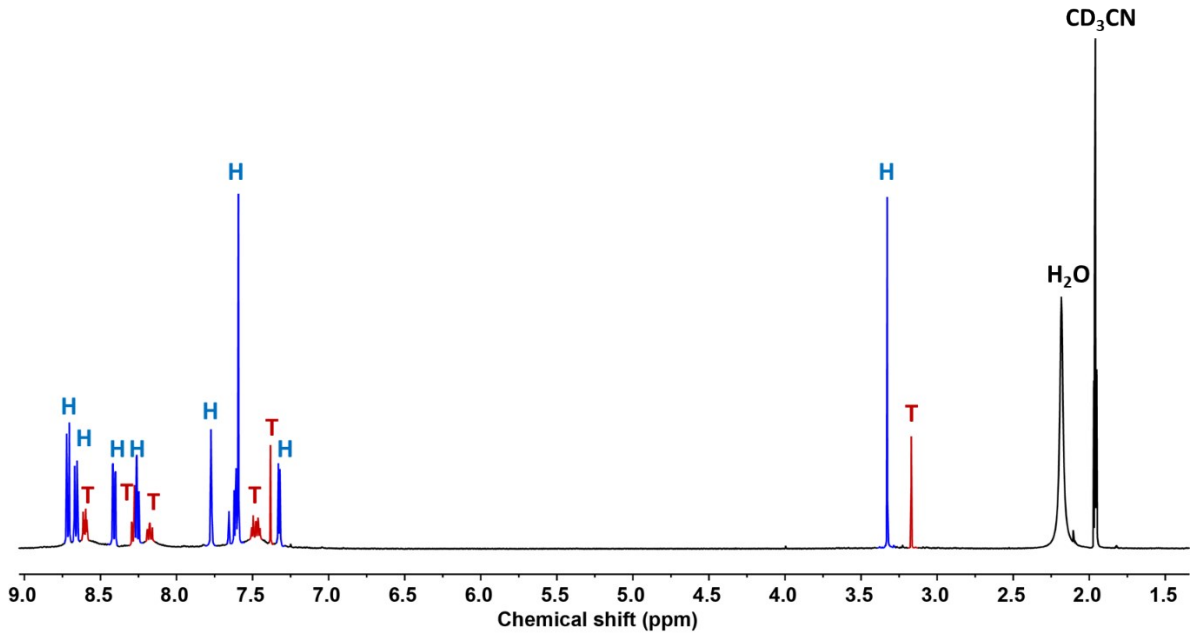

Figure S6. ^{1}H NMR spectrum (500 MHz, CD_3CN, 298K) of the mixture of $[Fe_2\mathbf{L}_3]\cdot 4PF_6$ (H) and $[Fe_4\mathbf{L}_6]\cdot 8PF_6$ (T).

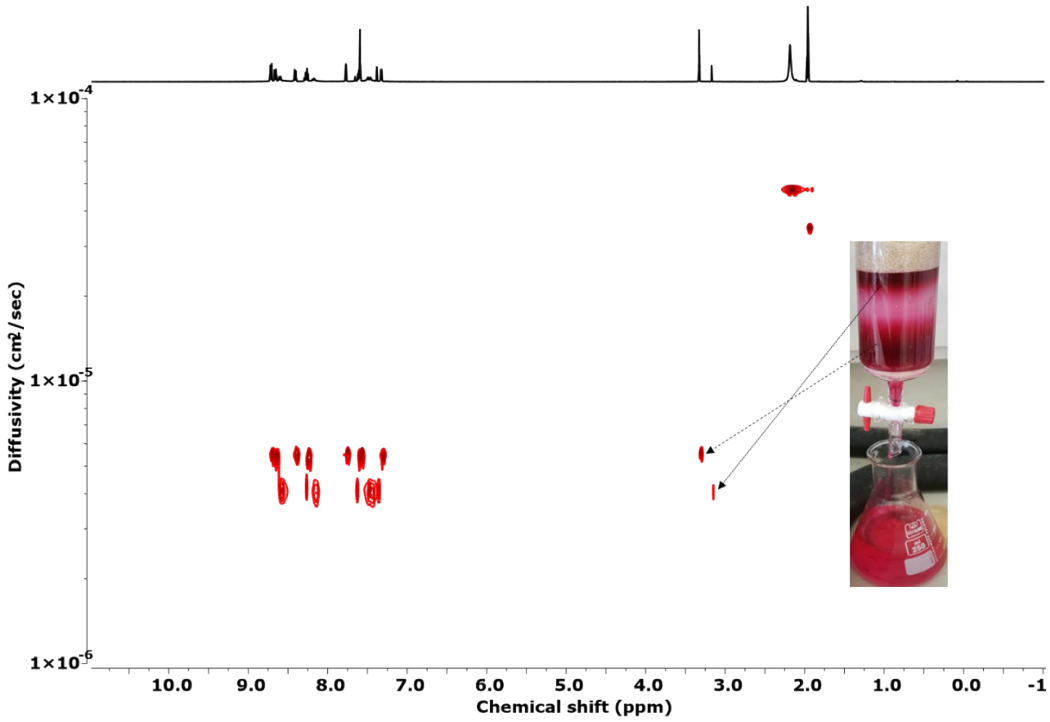

Figure S7. ^{1}H 2D DOSY NMR (500 MHz, CD_3CN, 298K) of the $[Fe_2\mathbf{L}_3]^{4+}$ and $[Fe_4\mathbf{L}_6]^{8+}$ mixture.

1.1.10 Synthesis of $[Fe_2\mathbf{L}_3]\cdot 4PF_6$ and $[Fe_4\mathbf{L}_6]\cdot 8PF_6\cdot 3MeCN\cdot 3MeOH$

The $[Fe_2\mathbf{L}_3]\cdot 4BF_4$ and $[Fe_4\mathbf{L}_6]\cdot 8BF_4$ reaction mixture was separated on silica gel using acetonitrile, water and saturated KNO_3 (7:1:0.5) as eluent two red products. Addition of excess saturated aqueous KPF_6 to the resulting fractions produced 97 mg (84 %) of helicate (first band) and 18 mg (16 %) tetrahedron (second band).

$[Fe_2(\mathbf{L})_3](PF_6)_4$: ^{1}H NMR(500 MHz, CD_3CN, δ/ppm, J/Hz): 8.75-8.71 (d, 2H^f, 6.2 Hz), 8.70-8.65 (m, 2H^e), 8.44-8.40 (dd, 2H^d, 8.4, 1.9 Hz), 8.30-8.24 (dt, 2H^c, 7.8, 1.4 Hz), 7.80-7.75(d, 2H^h, 2.0 Hz), 7.68-7.54 (m, 2H^a and 2H^i), 7.36-7.31(m, 2H^g), 3.27 (s, 2H^j). Positive ion ESI-HRMS: m/z (M= $[Fe_2(C_{30}H_{18}N_4)_3](PF_6)_4$ in acetonitrile); calculated $(M\text{-}2PF_6)^{2+}$ m/z = 852.6335, found m/z = 852.63; calculated $(M\text{-}3PF_6)^{3+}$ m/z = 520.1009, found m/z = 520.10; calculated $(M\text{-}4PF_6)^{4+}$ m/z = 353.8346, found m/z = 353.83.

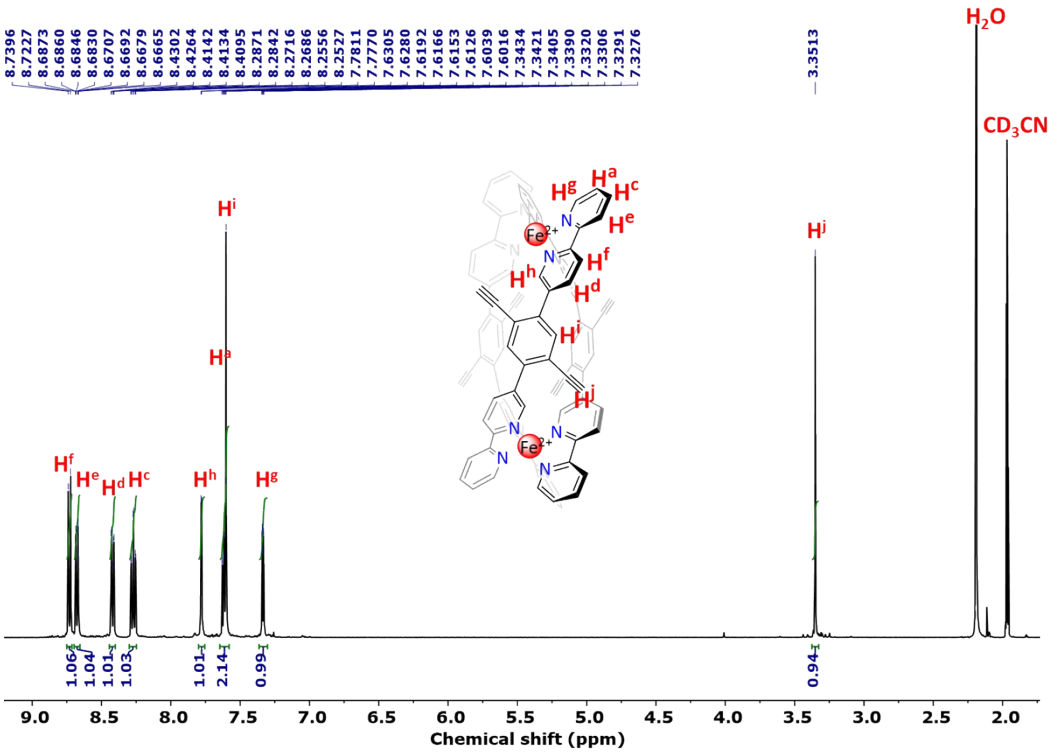

Figure S8. ^{1}H NMR spectrum (500 MHz, CD_3CN, 298K) of the $[Fe_2\mathbf{L}_3]\cdot 4PF_6$.

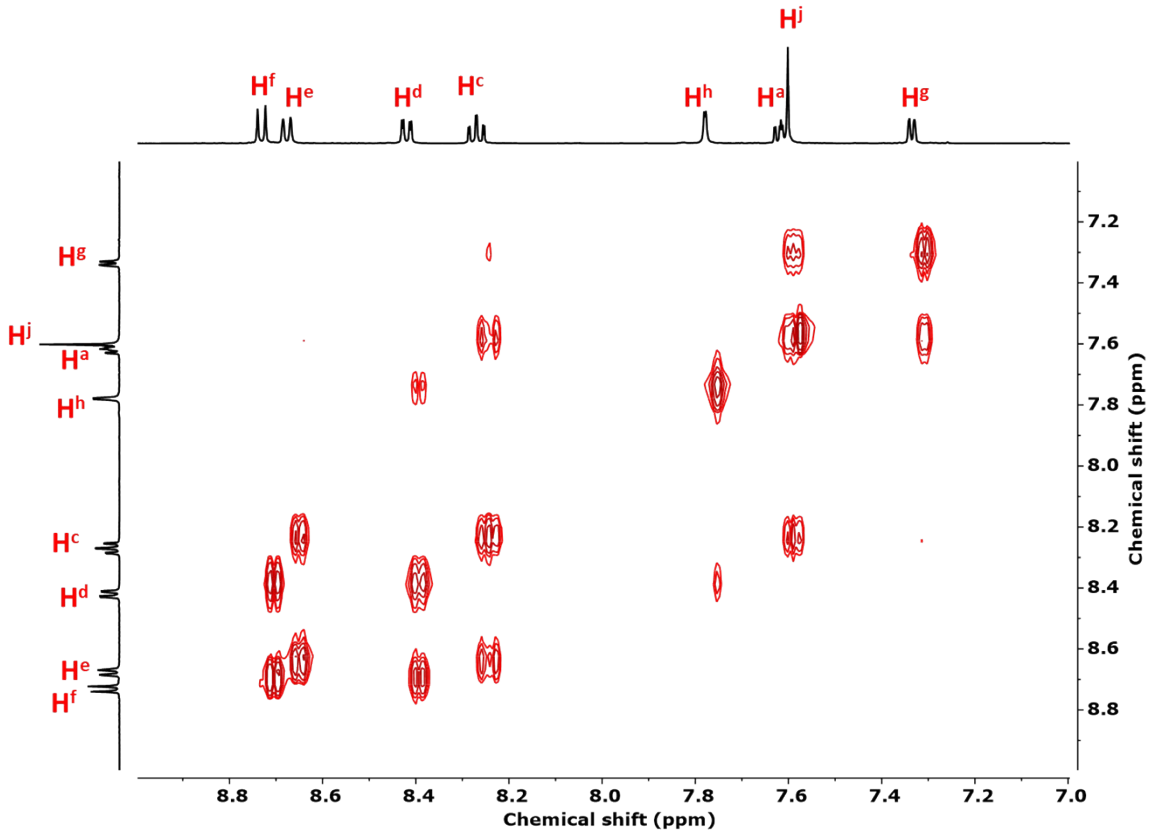

Figure S9. ^{1}H-^{1}H COSY spectrum (CD_3CN, 500 MHz, 298K) of $[Fe_2\mathbf{L}_3]\cdot 4PF_6$.in the aromatic region.

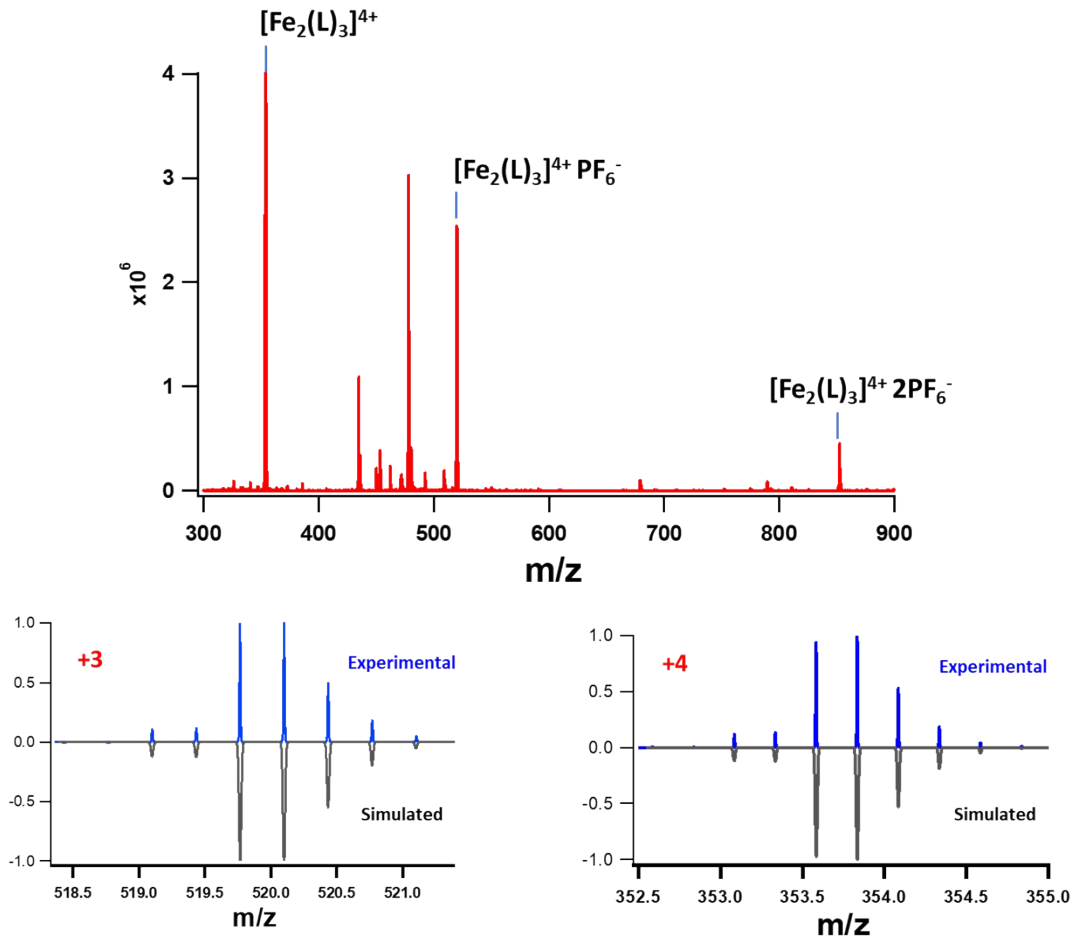

Figure S10. ESI-MS of the product +2, +3 and +4 ions detected that correspond to 2, 3 and 4 losses of PF_6^- ions from an $[Fe_2\mathbf{L}_3]\cdot 4PF_6$.

$[Fe_4\mathbf{L}_6]\cdot 8PF_6\cdot 3MeCN\cdot 3MeOH$: ^{1}H NMR (500 MHz, CD_3CN, δ/ppm, J/Hz): 8.64-8.58 (m, $2H^f$ and $2H^e$), 8.32-8.27 (dd, $2H^d$, 8.4, 2.0 Hz), 8.21-8.15 (dt, $2H^c$, 8.2, 1.6 Hz), 7.69-7.65 (dd, $2H^h$, 2.0, 0.7 Hz), 7.53-7.45 (m, $2H^g$ and $2H^a$), 7.39 (s, $2H^i$), 3.18(s, $2H^j$). ^{19}F NMR (470 MHz, CD_3CN) δ -72.71 (d, J = 707.3 Hz). Positive ion ESI-HRMS: m/z (M= $[Fe_4(C_{30}H_{18}N_4)_6](PF_6)_8$ in acetonitrile); calculated $(M\text{-}3PF_6)^{3+}$ m/z = 1184.8327, found m/z = 1184.83; calculated $(M\text{-}4PF_6)^{4+}$ m/z = 852.3835, found m/z = 852.38; calculated $(M\text{-}5PF_6)^{5+}$ m/z = 652.9139, found m/z = 652.91, calculated $(M\text{-}6PF_6)^{6+}$ m/z = 519.9342, found m/z = 519.93; calculated $(M\text{-}7PF_6)^{7+}$ m/z = 424.9487, found m/z = 424.95; calculated $(M\text{-}8PF_6)^{8+}$ m/z = 353.7096, found m/z = 353.71.

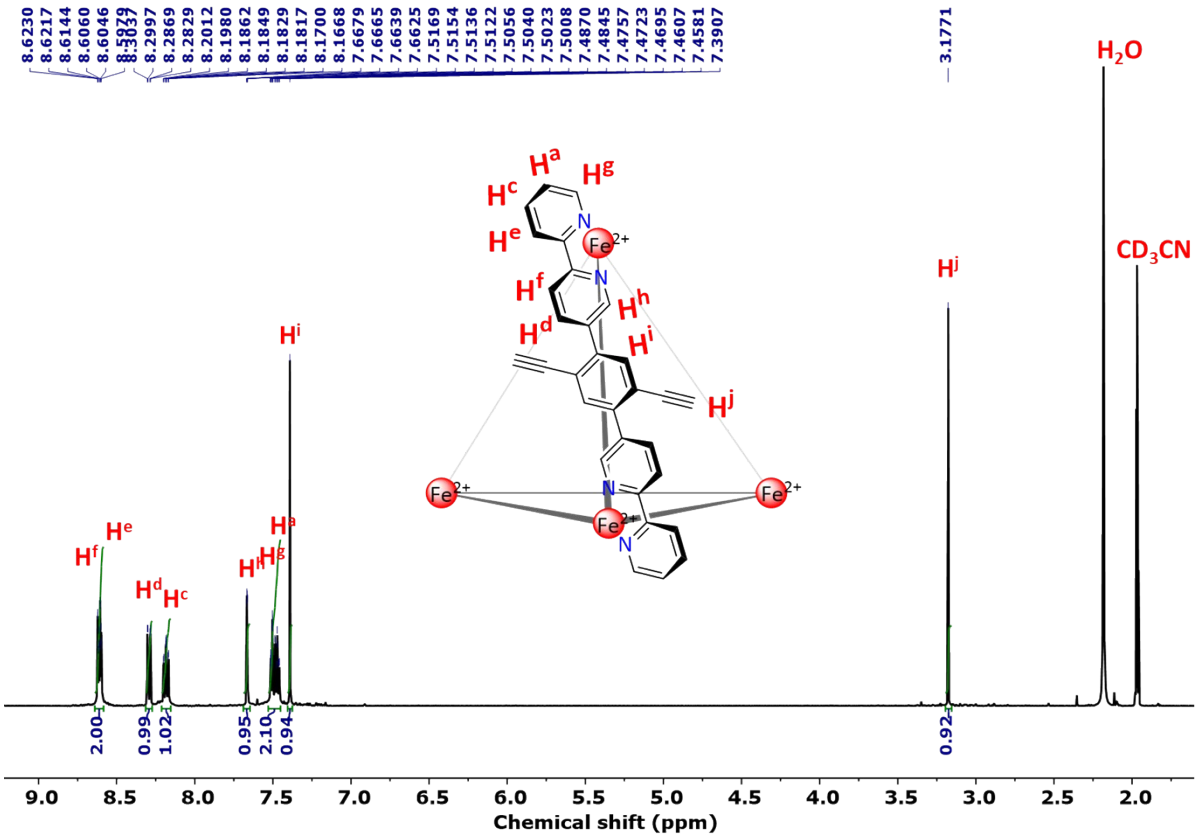

Figure S11. ^{1}H NMR spectrum (CD_3CN, 500 MHz, 298K) of $[Fe_4\mathbf{L}_6]\cdot 8PF_6$.

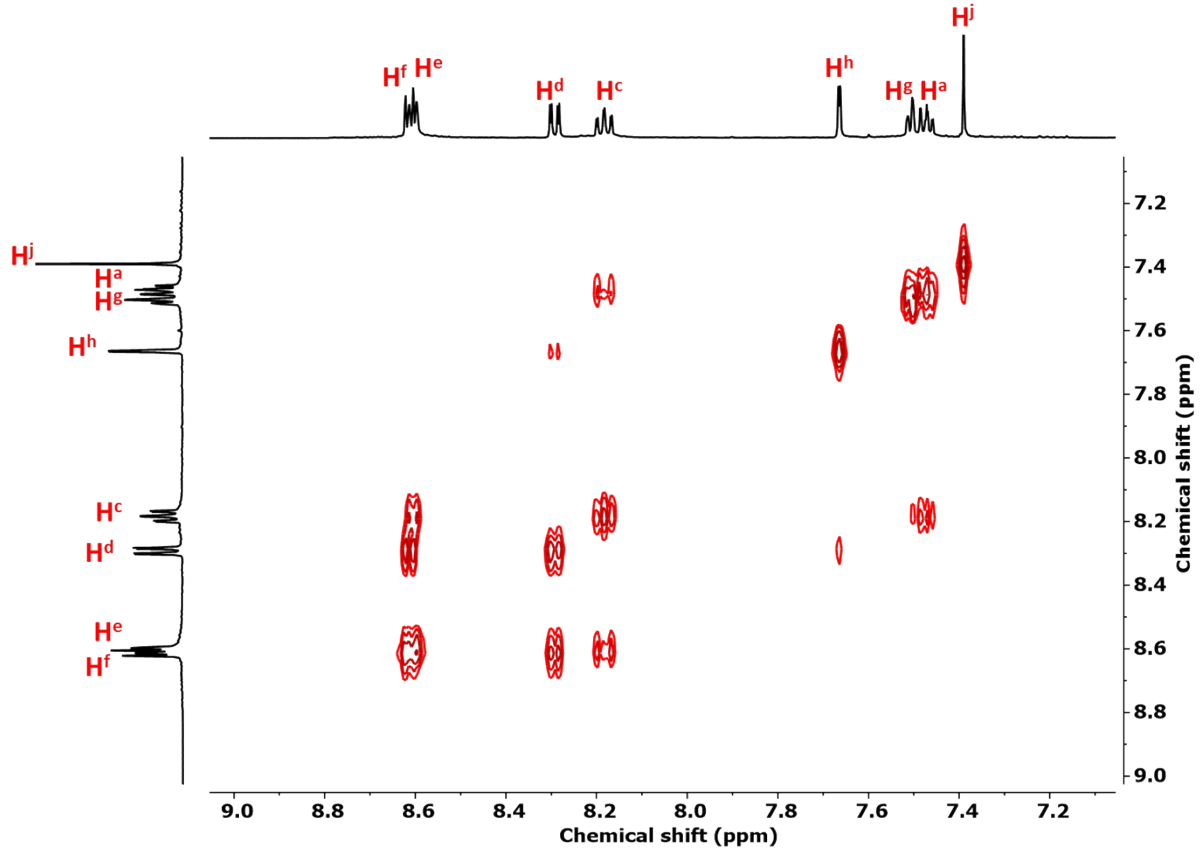

Figure S12. ^{1}H-^{1}H COSY spectrum (CD_3CN, 500 MHz, 298K) of $[Fe_4\mathbf{L}_6]\cdot 8PF_6$ in the aromatic region.

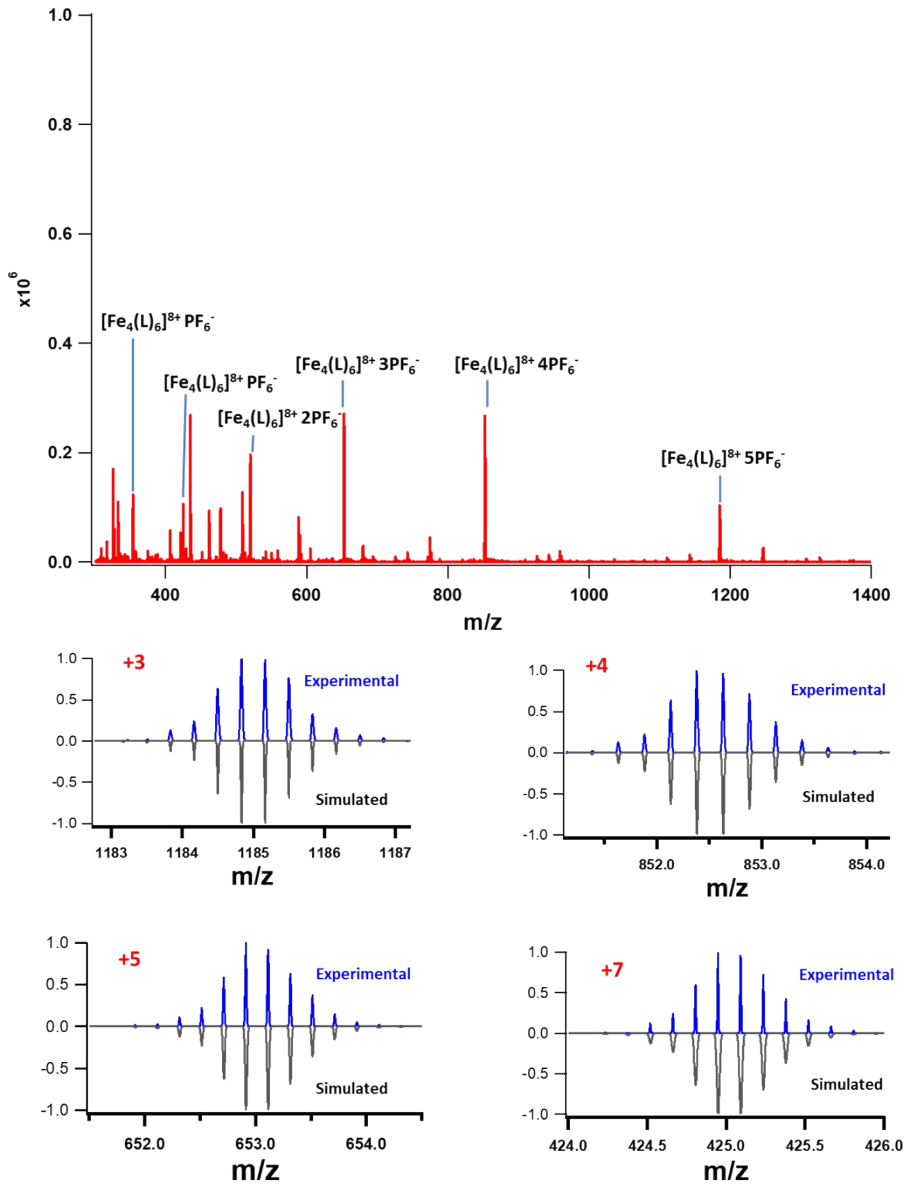

Figure S13. ESI-MS of the product +3, +4, +5, +6, +7 and +8 ions detected that correspond successive losses of PF_6^- ions from $[Fe_4\mathbf{L}_6]\cdot 8PF_6$.

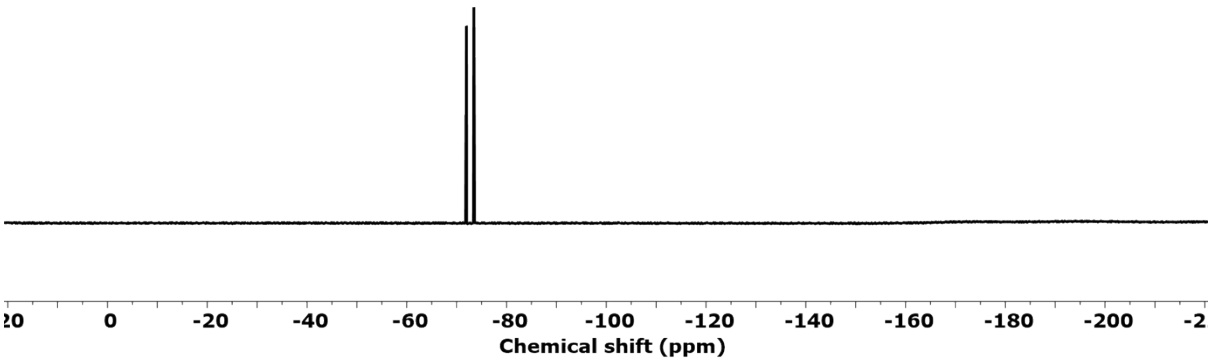

Figure S14. ^{19}F NMR spectrum (CD_3CN, 470 MHz, 298K) for $[Fe_4\mathbf{L}_6]\cdot 8PF_6$.

1.1.11 Synthesis of $[Fe_4(\mathbf{L}')_6](BF_4)$

The ligand $\mathbf{L}'$ (41.2 mg, 0.105 mmol) and $Fe(BF_4)_2.6H_2O$ (24mg, 0.07 mmol) were mixed in acetonitrile (10 mL) and the reaction mixture was heated in microwave for 30 minutes at 130 °C before heating overnight at 343 K.

$[Fe_4(\mathbf{L}')_6](BF_4)_8$ ^{1}H NMR (500 MHz, CD_3CN, δ/ppm, J/Hz): 8.71-8.64 (d, $2H_E$, 8.2 Hz), 8.63-8.57 (d, $2H_D$, 8.1 Hz), 8.47-8.39 (d, $2H_F$, 7.9 Hz), 8.18-8.08 (td, $2H_C$, 8.1, 1.0 Hz), 7.54-7.49 (m, $2H_A$ and $2H_G$),7.46-7.40 (m, $2H_B$), 7.28 (s, $4H_H$). Positive ion ESI-HRMS: m/z (M= $[Fe_4(\mathbf{L}')_6](BF_4)_8$ in acetonitrile); calculated $(M-2BF_4)^{3+}$ m/z = 1531.35, found m/z = 1531.35; calculated $(M-3BF_4)^{3+}$ m/z = 991.90, found m/z = 991.90; calculated $(M-4BF_4)^{4+}$ m/z = 722.42, found m/z = 722.42; calculated $(M-5BF_4)^{5+}$ m/z = 560.53, found m/z = 560.53, calculated $(M-6BF_4)^{6+}$ m/z = 452.61, found m/z = 452.61; calculated $(M-7BF_4)^{7+}$ m/z = 375.52, found m/z = 375.52; calculated $(M-8BF_4)^{8+}$ m/z = 317.70, found m/z = 317.70. The ^{1}H 2D DOSY NMR (500 MHz, CD_3CN, δ/ppm) of $[Fe_4(\mathbf{L}')_6](BF_4)_8$: Recorded diff con. for assigned peaks $4.45e^{-10}$ m^2s^{-1}; Calculated hydrodynamic radius 14.7Å.

To the resulting solution was then added saturated aqueous KPF_6 to yield the corresponding PF_6^- salt $[Fe_4(\mathbf{L}')_6](PF_6)_8$. ^{1}H NMR (500 MHz, CD_3CN, δ/ppm, J/Hz): 8.68-8.64 (d, $2H_E$, 8.5 Hz), 8.61-8.57 (d, $2H_D$, 8.2), 8.46-8.41(dd, $2H_F$, 8.5, 2.0 Hz), 8.15-8.09 (td, $2H_C$, 7.8, 1.3), 7.53-7.50 (d, $2H_A$, 5.1 Hz), 7.50-7.48 (d, $2H_G$, 1.8 Hz), 7.45-7.41(m, $2H_B$), 7.28 (s, $4H_H$).
^{19}F NMR (470 MHz, CD_3CN, δ/ppm) δ -72.71 (d, J = 707.3 Hz).

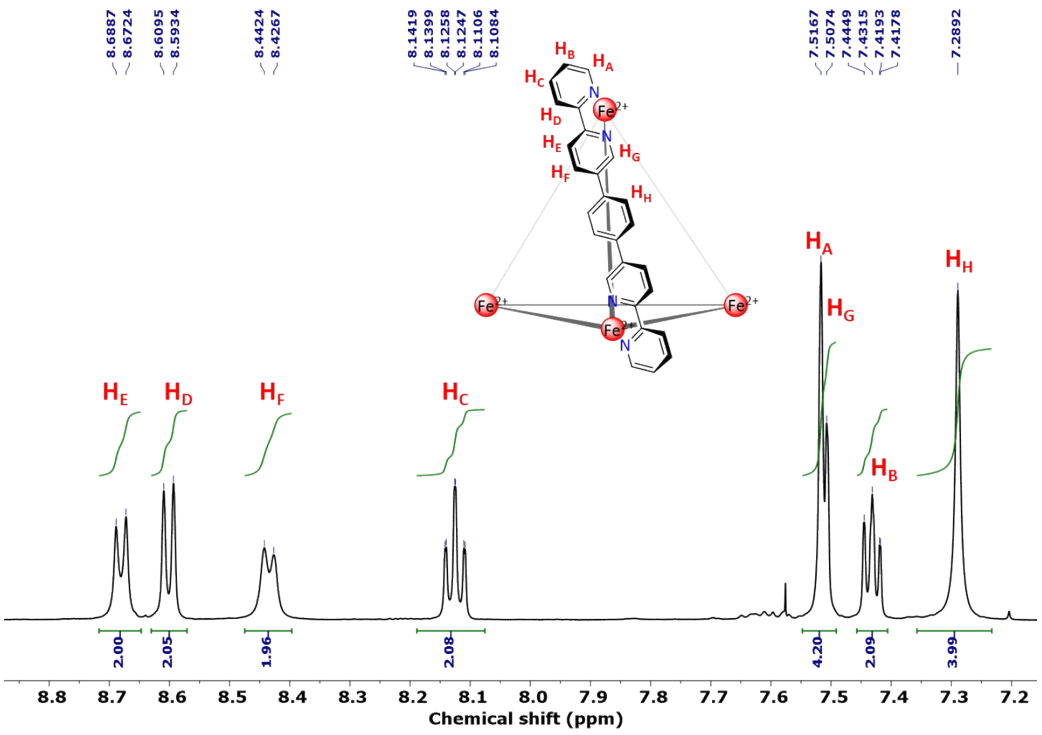

Figure S15. ^{1}H NMR spectrum (500 MHz, CD_3CN, 298K) of $[Fe_4\mathbf{L'}_6]\cdot 8BF_4$.

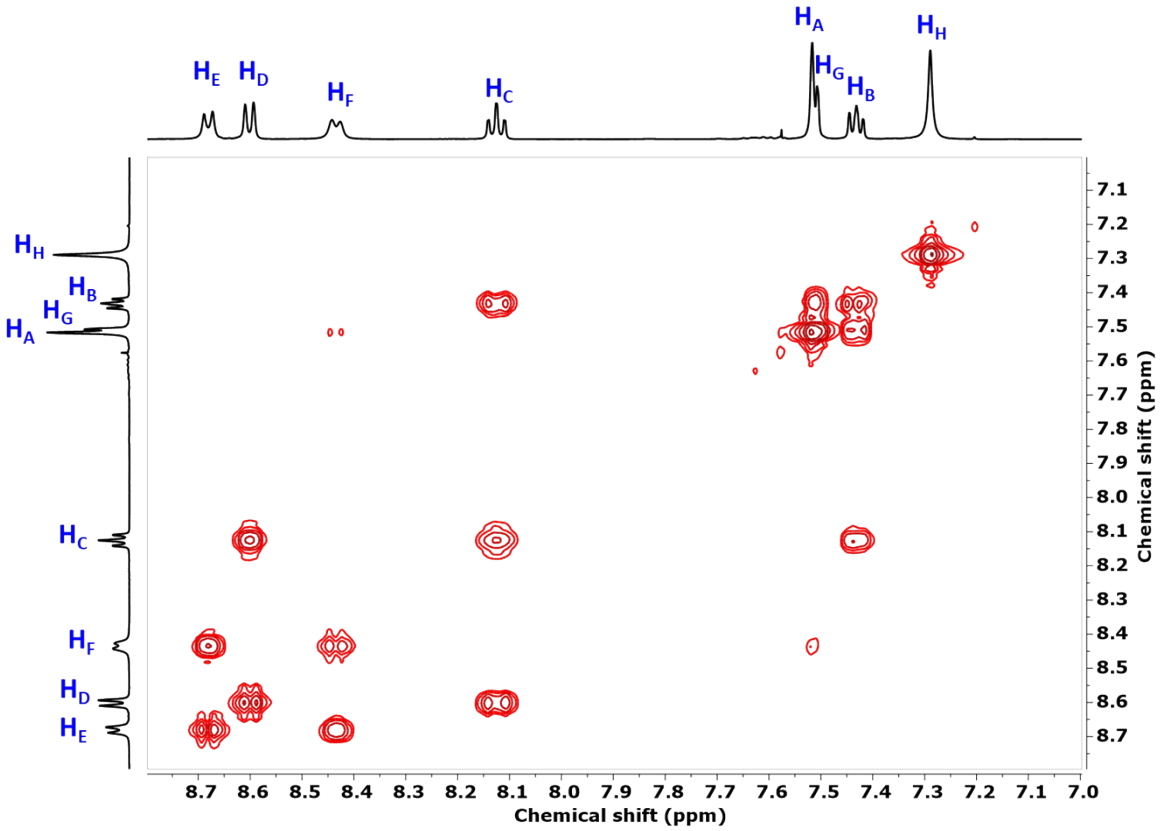

Figure S16. ^{1}H-^{1}H COSY spectrum (CD_3CN, 500 MHz, 298K) of $[Fe_4\mathbf{L'}_6]\cdot 8BF_4$ in the aromatic region.

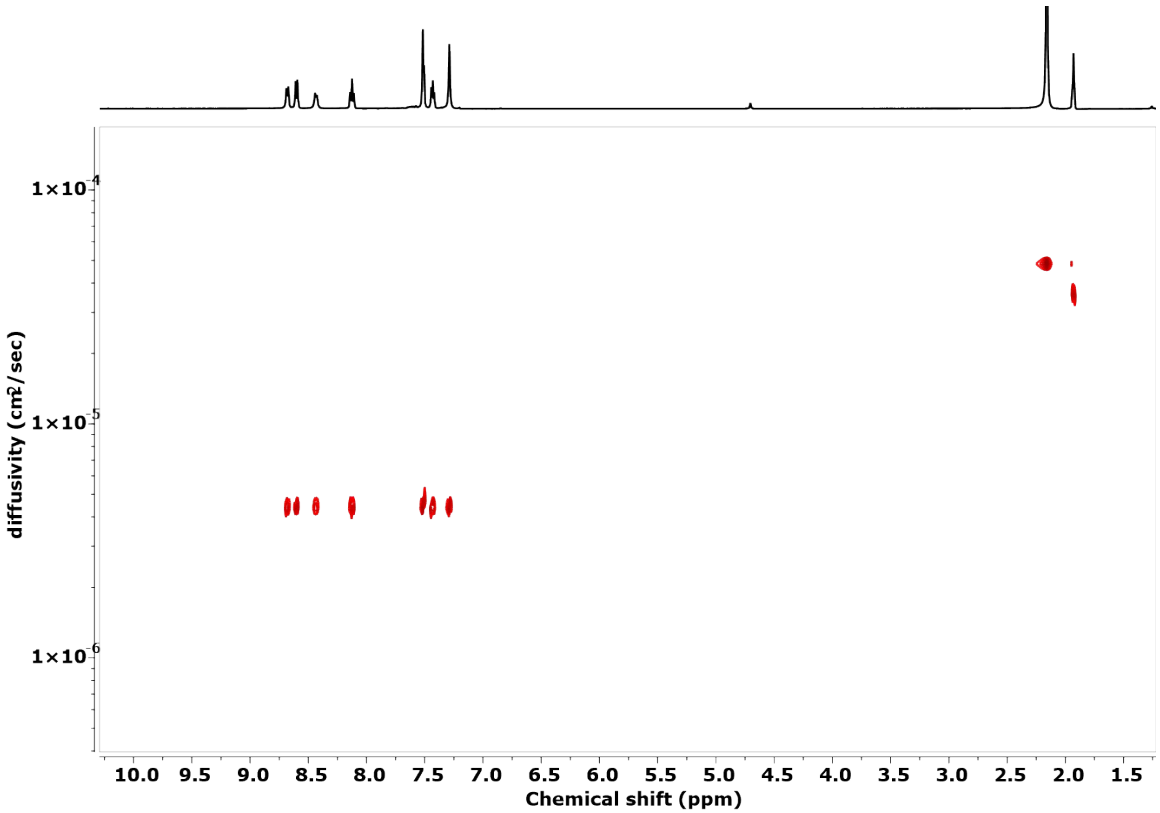

Figure S17. ^{1}H 2D DOSY NMR (500 MHz, CD_3CN, 298K) of the $[Fe_4\mathbf{L'}_6]\cdot 8BF_4$.

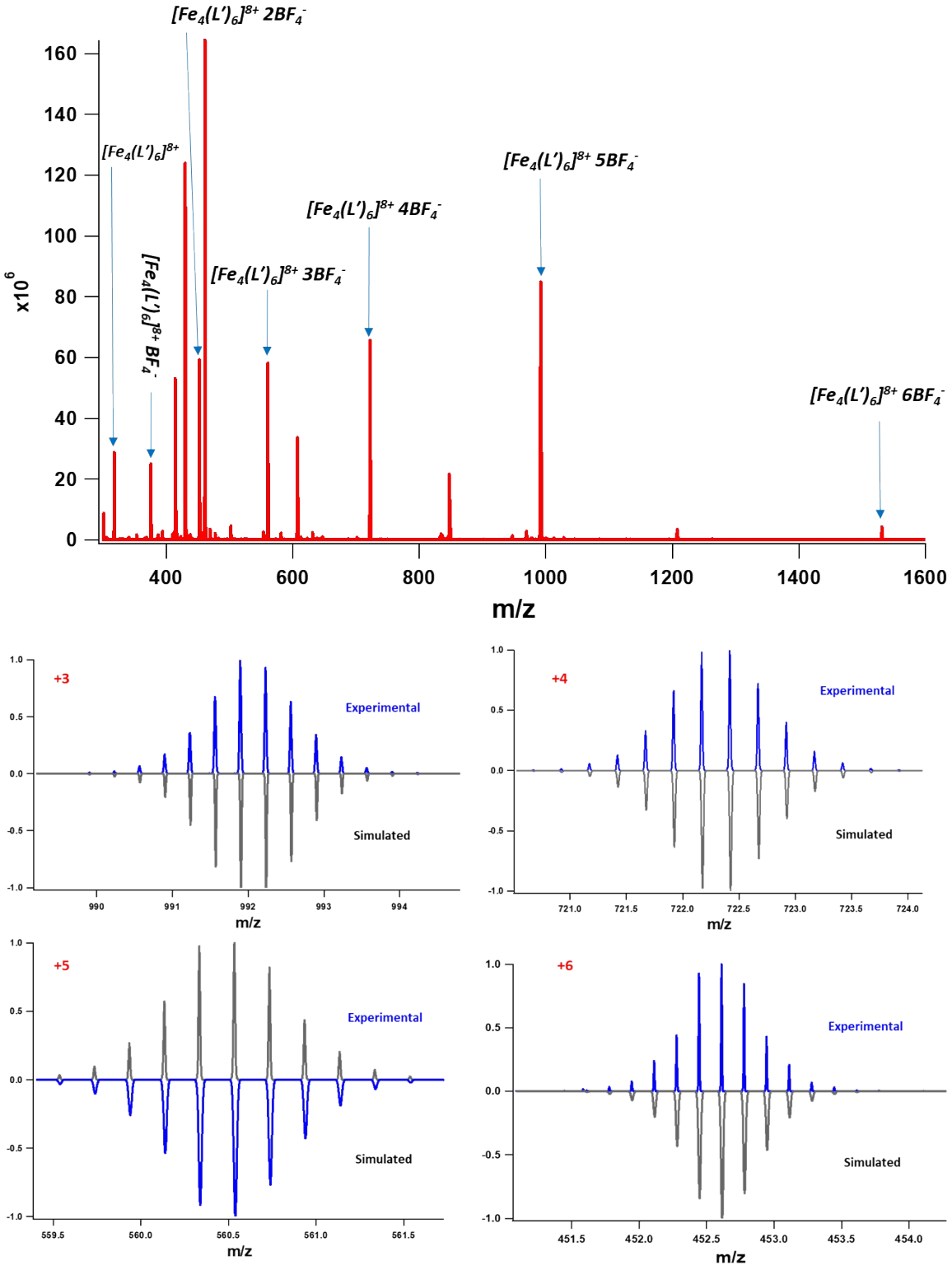

Figure S18. ESI-MS of the product +3, +4, +5, +6, +7 and +8 ions detected that correspond successive losses of BF_4^- ions from $[Fe_4\mathbf{L'}_6]\cdot 8BF_4$.

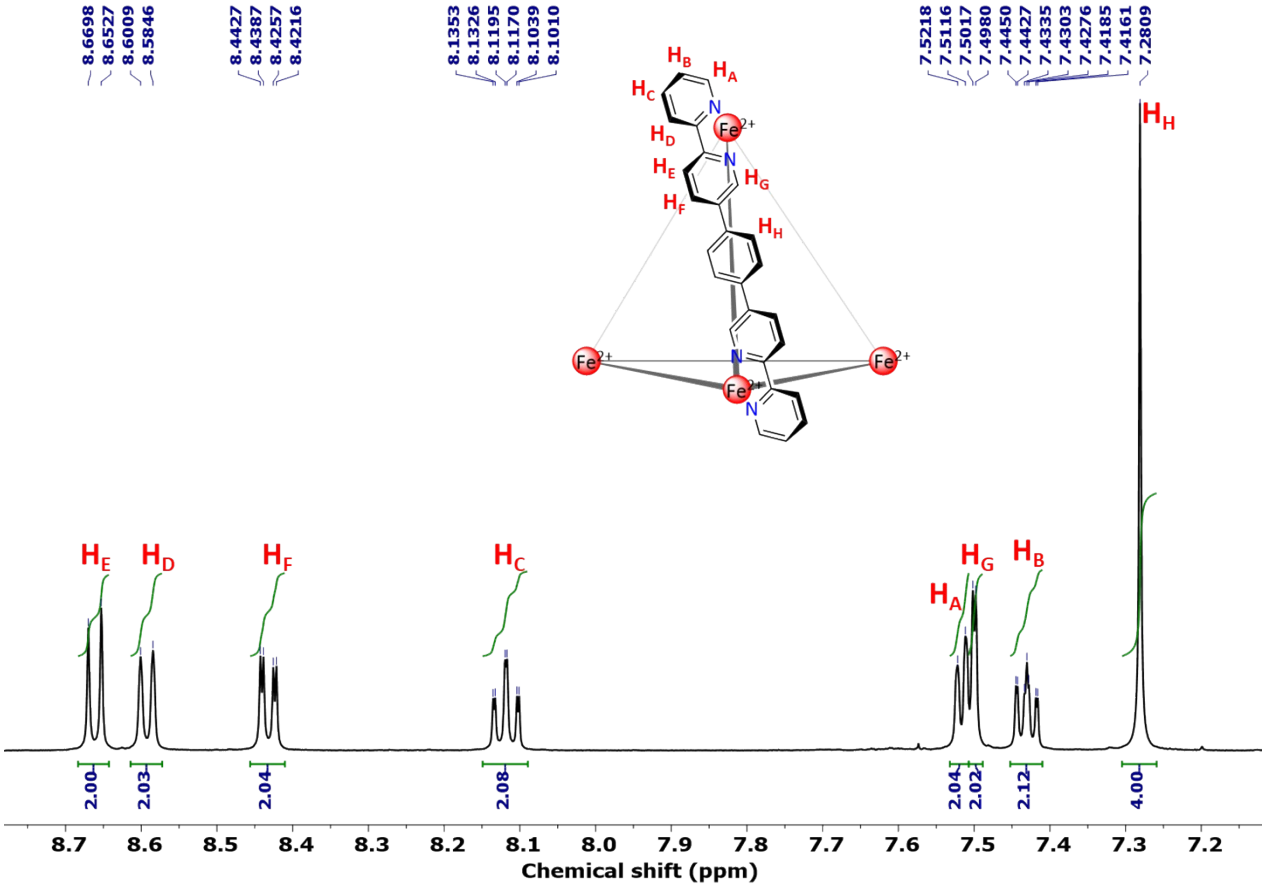

Figure S19. ^{1}H NMR spectrum (500 MHz, CD_3CN, 298K) of $[Fe_4\mathbf{L'}_6]\cdot 8PF_6$.

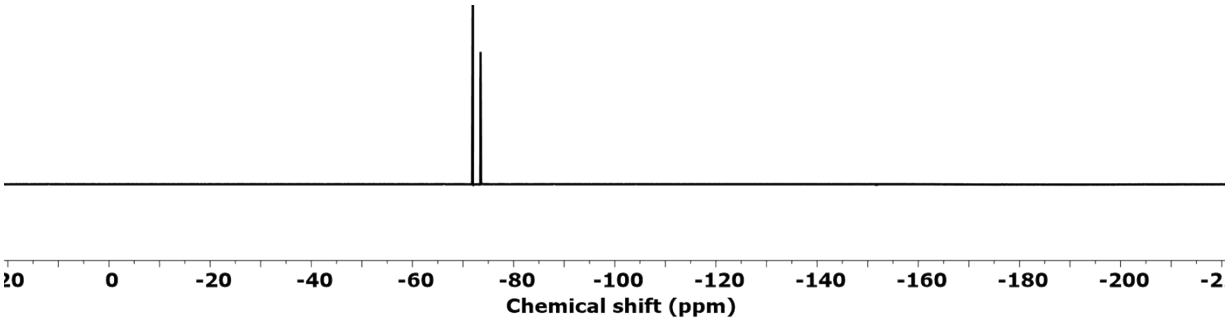

Figure S20. ^{19}F NMR spectrum (CD_3CN, 470 MHz, 298K) for $[Fe_4\mathbf{L'}_6]\cdot 8PF_6$.

1.2 Crystallography

Data were collected at the MX1 beamline of the Australian synchrotron with silicon double crystal monochromated radiation (0.7108 Å) at 100 K.[7] Data were processed with XDS.[8] Processed data was solved using SHELXT[9] within the Olex2[10] graphical interfaces. Solutions were refined via a full-matrix least-squares refinement against F2 using SHELXL-2018.[11] In general, non-hydrogen atoms with occupancies greater than 0.5 were refined anisotropically. Carbon-bound hydrogen atoms were included in idealized positions and refined using a riding model. Crystallographic data along with specific details pertaining to the refinement (inclusively addressing CheckCIF alerts), where required, follow.

*1.2.1 X-ray data for **5***

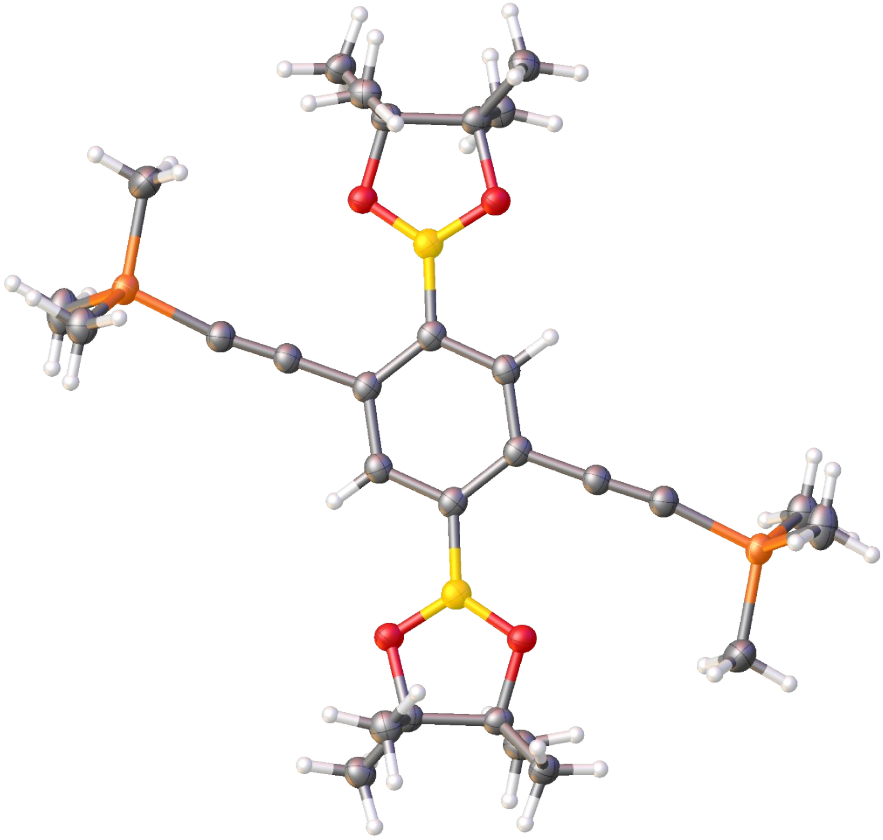

Figure S21. Crystal structure of **5**.

X-ray quality crystals of **5** were grown by the slow evaporation of ethyl acetate. It crystallised in monoclinic $P2_1/n$ and the asymmetric unit consists of one half of the molecule. The closest contact between the two molecules is through weak interaction of oxygen of pinacol ester of one molecule and the methyl hydrogen of TMS-acetylene of the second molecule.

Formula $C_{28}H_{44}B_2O_4Si_2$, M = 522.43, monoclinic, space group $P2_1/n$, a = 10.673(2), b = 10.211(2), c = 15.278(3), α = 90°, β = 110.38(3)°, γ = 90° V = 1560.9(6)Å^3, D_c = 1.112 g cm^{-3}, Z = 2, crystal size 0.08 × 0.06 × 0.03 mm, colour colourless, habit plate, temperature = 100(2) K, λ(Synchrotron) = 0.7108 Å, μ(Synchrotron) = 0.143 mm^{-1}, $2\theta_{max}$ = 50.44, hkl range -12 to 12, -12 to 9, -18 to 18, N = 15114, N_{ind} = 2749 (R_{merge} 0.0746), R_1(F) 0.0606, $wR2$(F^2 , all) 0.1860, GoF(all) 1.146, D$\rho_{min,max}$ 0.40/-0.56 e$^-$ Å^{-3}.

1.2.2 X-ray data for ***6***

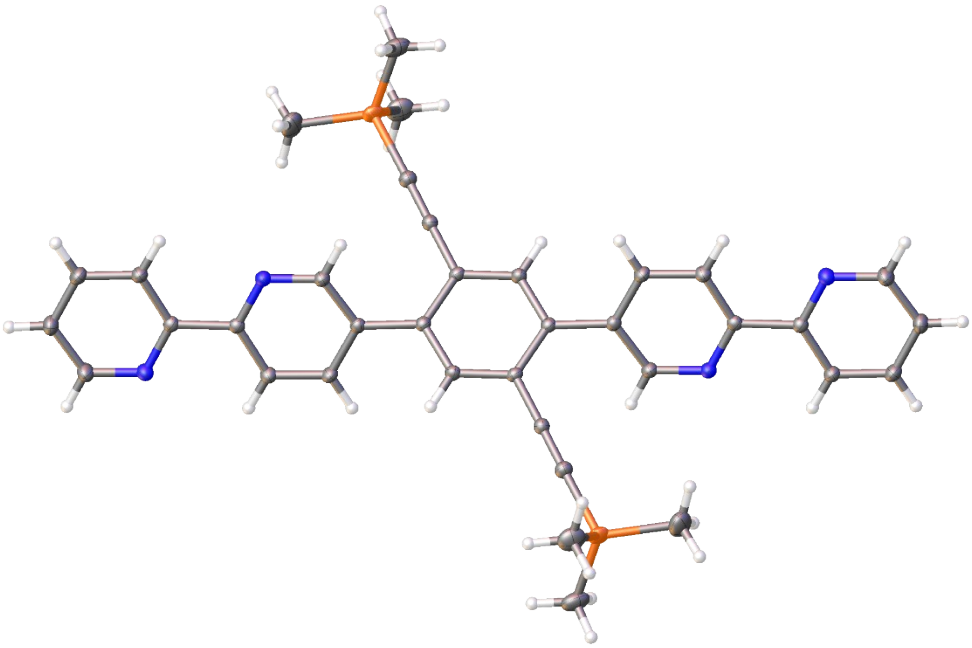

Figure S22. Crystal structure of **6**.

Colourless needles suitable for X-ray diffraction were grown from ethyl acetate by slow evaporation. **6** crystallised in monoclinic $P2_1/c$ and the asymmetric unit contains half a molecule of ligand. Due to steric interference of trimethyl silyl groups on both sides of the ligands, no π-π stacking is observed. The closest contact between the two molecules is through non-classical hydrogen bonding.

Formula $C_{36}H_{34}N_4Si_2$, M = 522.43, monoclinic, space group $P2_1/c$, a = 7.3560(15), b = 15.326(3), c = 14.709(3), α = 90°, β = 99.74(3)°, γ = 90° V = 1634.4(6)Å^3, D_c = 1.176 g cm^{-3}, Z = 2, crystal size 0.07×0.03×0.02 mm, colour colourless, habit plate, temperature = 100(2) K, λ(Synchrotron) = 0.7108 Å, μ(Synchrotron) = 0.143 mm^{-1}, $2\theta_{max}$ = 56.556, hkl range -9 to 9,

-19 to 19, -19 to 19, $N = 26585$, $N_{ind} = 3917$ (R_{merge} 0.0555), R_1(F) 0.0506, $wR2(F^2$, all) 0.1461, GoF(all) 1.063, $D\rho_{min,max}$ 0.38/-0.64 e^- Å^{-3}.

1.2.3 X-ray data for ***L***

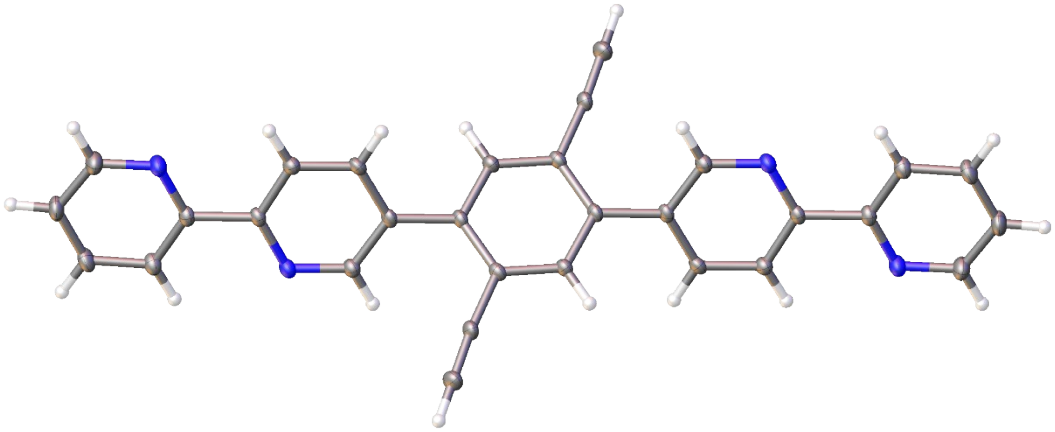

Figure S23. Crystal structure of **L**.

The crystals suitable for diffraction were grown from chloroform by slow evaporation. **L** crystallised in *Pbca* and the asymmetric unit consists of half a molecule of ligand. The molecules are more closely packed than in **6** and offset π-π stacking is observed. Additionally, non-classical hydrogen bonding also exists between nitrogens of the pyridyl group and proton either from the acetylene or the aromatic ring.

Formula $C_{30}H_{18}N_4$, $M = 434.48$, orthorhombic, space group *Pbca*, $a = 11.112(2)$, $b = 12.500(3)$, $c = 15.599(3)$, $\alpha = \beta = \gamma = 90^o$, $V = 2166.7(7)$ Å^3, $D_c = 1.332$ g cm^{-3}, $Z = 2$, crystal size 0.05 × 0.03 × 0.02 mm, colour colourless, habit plate, temperature = 100(2) K, λ(Synchrotron) = 0.7108 Å, μ(Synchrotron) = 0.08 mm^{-1}, $2\theta_{max} = 56.554$, hkl range -14 to 14, -16 to 16, -20 to 20, $N = 34421$, $N_{ind} = 2677$ (R_{merge} 0.0467), R_1(F) 0.0562, $wR2(F^2$, all) 0.1302, GoF(all) 1.078, $D\rho_{min,max}$ 0.46/-0.27 e^- Å^{-3}.

1.2.4 X-ray data for $[Fe_2\mathbf{L}_3]\cdot 4PF_6$

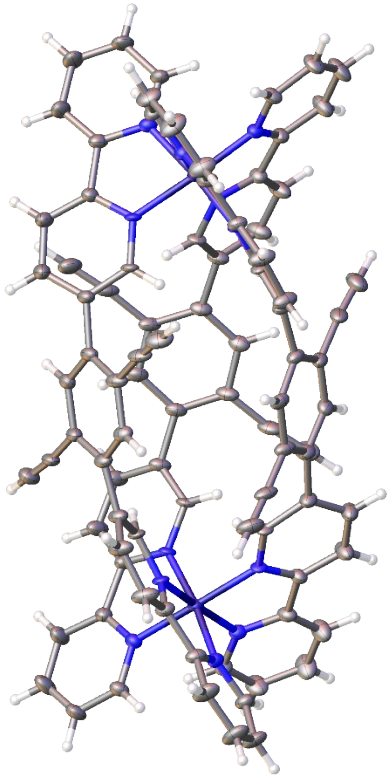

Figure S24. Crystal structure of $[Fe_2\mathbf{L}_3]\cdot 4PF_6$.

Crystals were grown by the slow diffusion of diethyl ether into an acetonitrile solution of the product. The helical complex crystallised in space group $P6_322$ and the asymmetric unit consists of one sixth of the assembly due to presence of three-fold and two-fold axes of rotation. The C_2-symmetric ligand **L** forms triple stranded helicate with two homochiral iron(II) ions ($\Delta\Delta$). A significant distortion in the planarity of the ligand can be seen in the helical assembly and the associated bend angle of the ligand in the helical assembly was defined from the centroid of central phenyl ring to the both ends of ligand and this bend is 36° to the metal centres and the chiral twist associated with the helix is 55° from the idealized *syn*-configuration.

Formula $C_{90}F_{24}Fe_2H_{54}N_{12}P_4$, M = 1995.03, hexagonal, space group $P6_322$, a = 13.4333(13), b = 13.4333(13), c = 27.740(6), α = 90°, β = 90°, γ = 120° V = 4335.1(12)Å^3, D_c = 1.528 g cm^{-3}, Z = 2, crystal size 0.09×0.06×0.03 mm, colour red, habit plate, temperature = 100(2) K, λ(Synchrotron) = 0.7108 Å, μ(Synchrotron) = 0.515 mm^{-1}, $2\theta_{max}$ = 56.562, hkl range -17 to 17, -17 to 17, -36 to 36, N = 73262, N_{ind} = 3604 (R_{merge} 0.0587), R_1(F) 0.0552, $wR2$(F^2 , all) 0.1880, GoF(all) 1.181, D$\rho_{min,max}$ 0.66/-0.43e$^-$ Å^{-3}.

Specific details: The crystals employed rapidly decay after removal from the mother liquor. Rapid (<1 min) handling at dry ice temperatures prior to quenching in the cryostream was required to collect data. Anions display high thermal motion indicating unresolved disorder and a number of bond length constraints were required to facilitate realistic modelling. In addition, reflecting the instability of the crystals, there is a large area of smeared electron density present in the lattice. Despite many attempts to model this region of disorder as a combination of solvent and anion molecules no reasonable fit could be found and accordingly this region was treated with the solvent mask function the Olex2.

*1.2.5 X-ray data for ([Fe$_4$**L**$_6$]·8PF$_6$·3MeCN·3MeOH)*

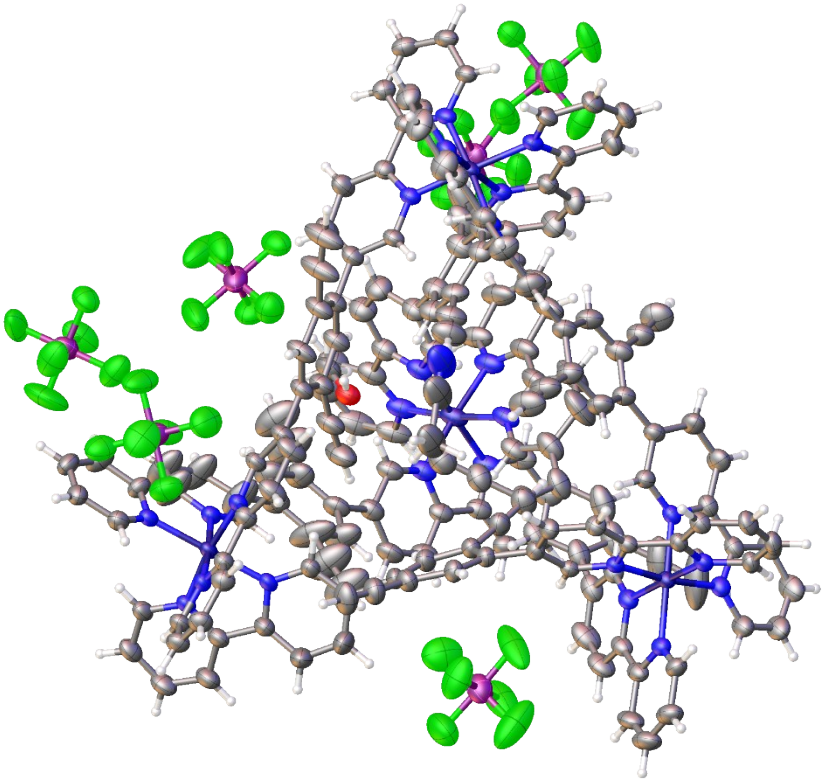

Figure S25. Crystal structure of ([Fe$_4$**L**$_6$]·8PF$_6$·3MeCN·3MeOH).

Crystals were grown by the slow diffusion of methanol into an acetonitrile solution of the product. Crystal structural analysis revealed that it crystallised in triclinic *P***Error!**. The asymmetric unit contains one complete unit of complex with eight PF_6^- counter-anion and solvent molecules. Both enantiomers (*ΔΔΔΔ* and *ΛΛΛΛ*) of the tetrahedron are related to each other through a centre of inversion (Figure S26). The Fe(II) centres lie an average of 13.20 Å apart which is a significantly longer distance than the 11.63 Å of the helical assembly.

Formula $C_{189}H_{129}F_{48}Fe_4N_{27}O_3P_8$, M = 4209.34, triclinic, space group *P-1*, a = 16.904(3), b = 22.714(5), c = 29.166(6), α = 78.57(3)°, β = 73.36(3)°, γ = 69.54(3)°, V = 9992(4)Å^3, D_c = 1.399 g cm^{-3}, Z = 2, crystal size 0.1 × 0.06 × 0.03 mm, colour red, habit plate, temperature = 100(2) K, λ(Synchrotron) = 0.7108 Å, μ(Synchrotron) = 0.452 mm^{-1}, $2\theta_{max}$ = 50.444, hkl range -20 to 20, -26 to 26, -34 to 34, N = 126810, N_{ind} = 32802 (R_{merge} 0.0768), R_1(F) 0.0662, *wR*2(F^2 , all) 0.2084, GoF(all) 1.040, D$\rho_{min,max}$ 1.07/-1.24e$^-$ Å^{-3}.

Specific details: The crystals employed rapidly lost solvent after removal from the mother liquor. Rapid (<1 min) handling at dry ice temperatures prior to quenching in the cryostream was required to collect data. Some of the anions display high thermal motion indicating unresolved disorder and a number of bond length constraints were required to facilitate realistic modelling. In addition, reflecting the instability of the crystals, there is a large area of smeared electron density present in the lattice. Despite many attempts to model this region of disorder as a combination of solvent and anion molecules no reasonable fit could be found and accordingly this region was treated with the solvent mask function the Olex2.

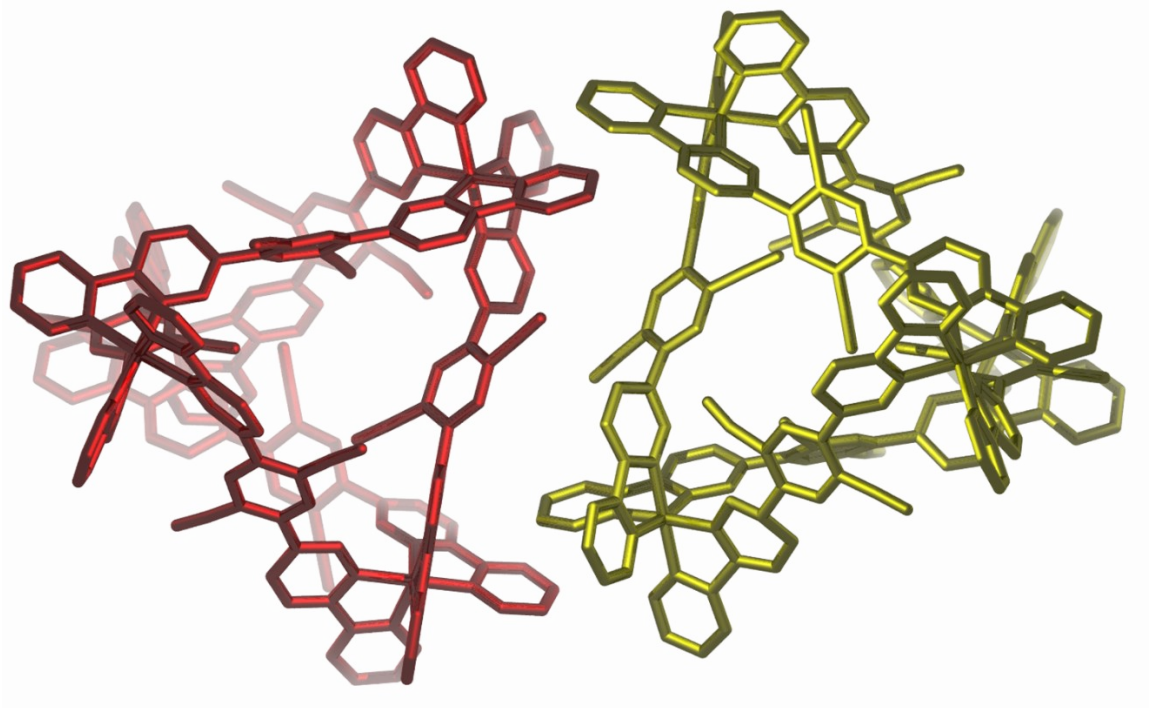

Figure S26. Dimeric packing of two enantiomeric tetrahedral *ΔΔΔΔ*- and *ΛΛΛΛ*-$[Fe_4\mathbf{L}_6]^{8+}$ cages which are related to each other through a centre of inversion.

*1.2.6 X-ray data for ([Fe_4**L'**$_6$]·8PF_6·4.5MeCN·3THF)*

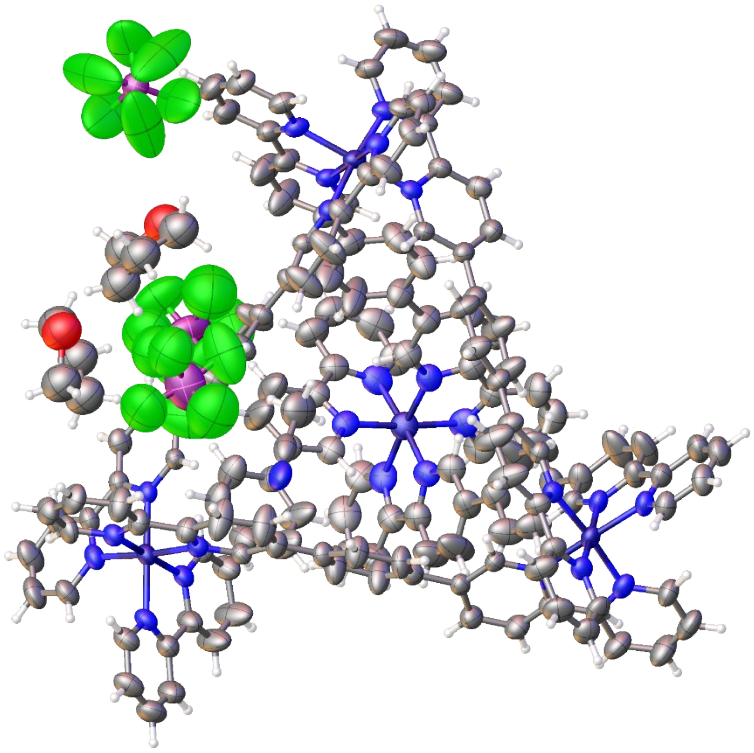

Figure S27. Crystal structure of [Fe_4**L′**$_6$]·8PF_6·4.5MeCN·3THF.

Red coloured plates suitable for X-ray diffraction were grown by slow diffusion of THF into solution of complex in acetonitrile. The crystal structure of the complex is shown in **Figure S27**. Crystal structural analysis revealed that it is indeed a tetrahedral assembly and it crystallised in the *P***Error!** space group. The asymmetric unit of complex contains only one-third of the molecule because it crystallized around three-fold axis. The cage exists as a racemic mixture of homoconfigurational *T*-symmetric tetrahedra (either *ΔΔΔΔ* or *ΛΛΛΛ*). The Fe(II) centres are separated by 13.23 Å and none of the PF_6^- anions were found to be encapsulated.

Formula $C_{177}H_{163.5}F_{48}Fe_4N_{28.5}O_3P_8$, M = 4102.87, trigonal, space group *P***Error!**, a = 21.2196(8), b = 21.2196(8), c = 30.9753(11), $\alpha = \beta = 90^o$, $\gamma = 120^o$, V = 12078.7(10) Å^3, D_c = 1.128 g cm^{-3}, Z = 2, crystal size 0.15 × 0.12 × 0.06 mm, colour red, habit plate, temperature = 100(2) K, λ(Mo Kα) = 0.71073 Å, $2\theta_{max}$ = 56.562, hkl range -28 to 28, -24 to 28, -41 to 40, N = 85859, N_{ind} = 19903 (R_{merge} 0.0665), R_1(F) 0.13, $wR2$(F^2 , all) 0.3394, GoF(all) 1.080, D$\rho_{min,max}$ 1.45/-1.07 e$^-$ Å^{-3}.

1.3 Interconversion of $[Fe_2L_3]^{4+}$ and $[Fe_4L_6]^{8+}$

1.3.1 ^{1}H NMR studies under ambient conditions

Initially, the dynamic behaviour of both assemblies was monitored by ^{1}H NMR at ambient conditions. In the first experiment, 15 mg of $[Fe_4\mathbf{L}_6]^{8+}$ (**T**) was dissolved in 0.8 mL CD_3CN and the ^{1}H NMR was recorded at regular intervals for 50 days.

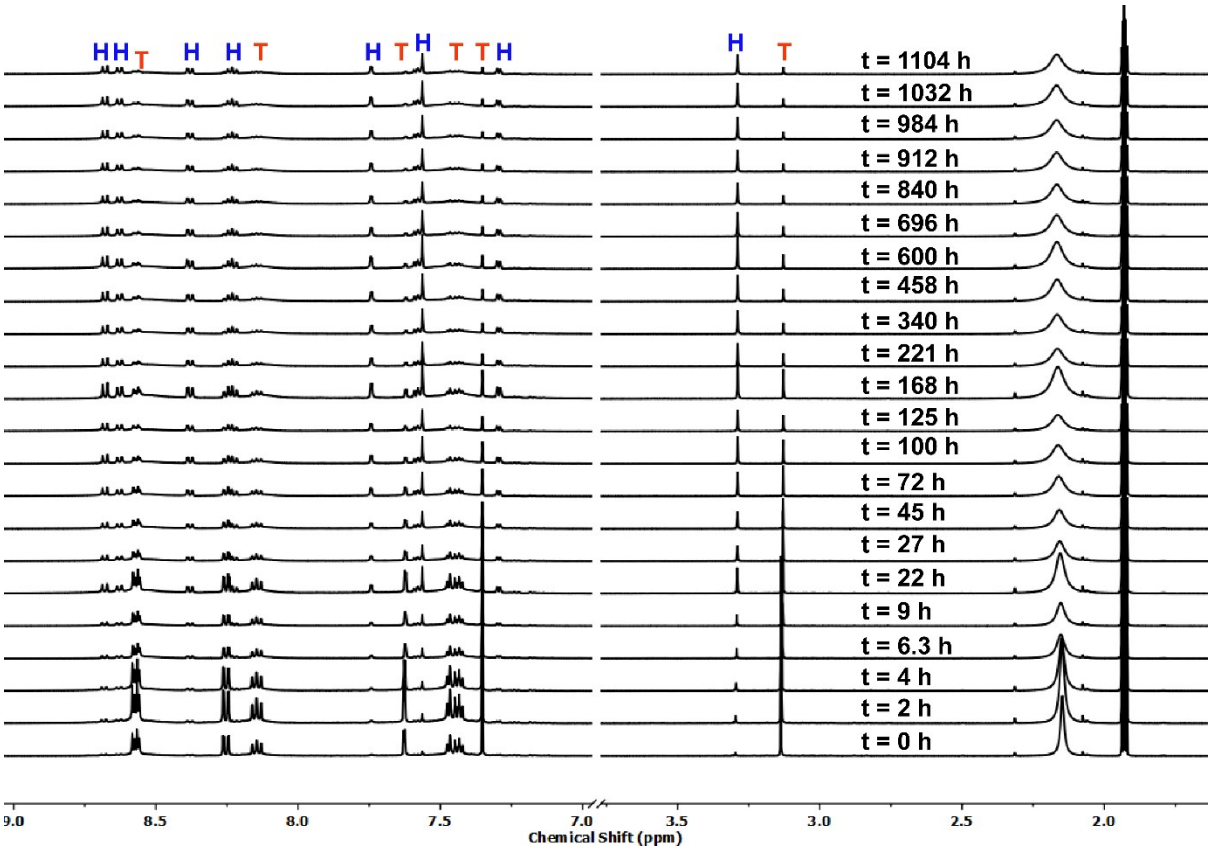

Figure S28. Selected ^{1}H NMR spectra (500 MHz, CD_3CN) showing the growth of the helical assembly from the tetrahedral assembly until equilibrium reached as function of time.

In a second experiment, 15 mg of $[Fe_2\mathbf{L}_3]^{4+}$ (**H**) was dissolved in 0.8 mL CD_3CN and the ^1H NMR was recorded at regular intervals for 50 days at ambient conditions.

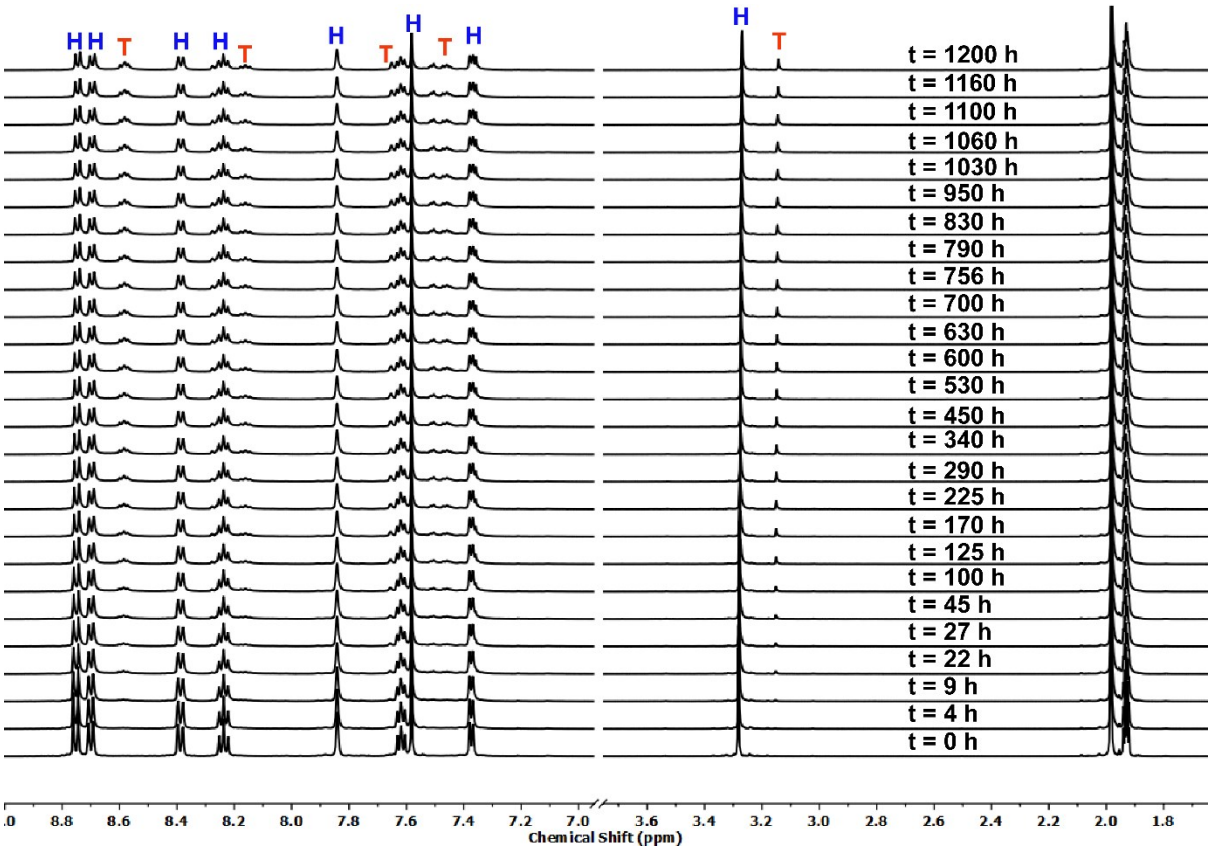

Figure S29. Selected ^1H NMR spectra (500 MHz, CD_3CN) showing the growth of the tetrahedral assembly from the helical assembly until equilibrium reached.

1.3.2 In situ ^{1}H NMR study of $[Fe_4\mathbf{L}_6]^{8+}$ at 343 K

15 mg of $[Fe_4\mathbf{L}_6]\cdot 8PF_6\cdot 3MeCN\cdot 3MeOH$ (**T**) was dissolved in 0.8 mL CD_3CN and the ^{1}H NMR spectra were acquired at 10 minute intervals at 343 K over 24 hrs *in-situ* in the NMR spectrometer (Figure S31). Based on acetylenic proton peak integrals of each assembly, the relative concentrations of each complex were determined.

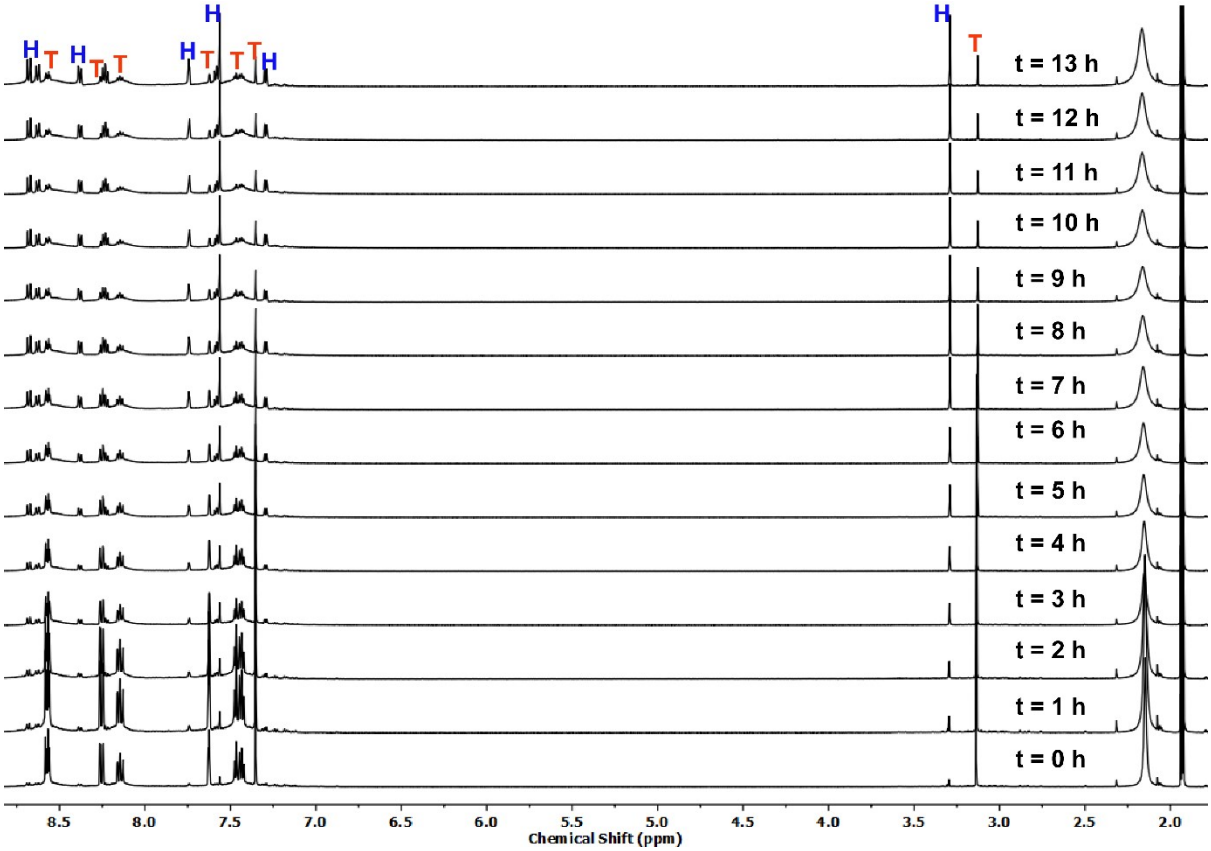

Figure S30. Selected ^{1}H NMR spectra (400 MHz, CD_3CN) showing the growth of the helical assembly from tetrahedron assembly as function of time at 343K.

1.3.3 In situ ^{1}H NMR study of $[Fe_2\mathbf{L}_3]^{8+}$ at 343 K

15 mg of $[Fe_2\mathbf{L}_3]\cdot 4PF_6$ (**H**) was dissolved in 0.8 mL CD_3CN and the ^{1}H NMR spectra were acquired at 10 minute intervals at 343 K over 14 hrs *in-situ* in the NMR spectrometer.

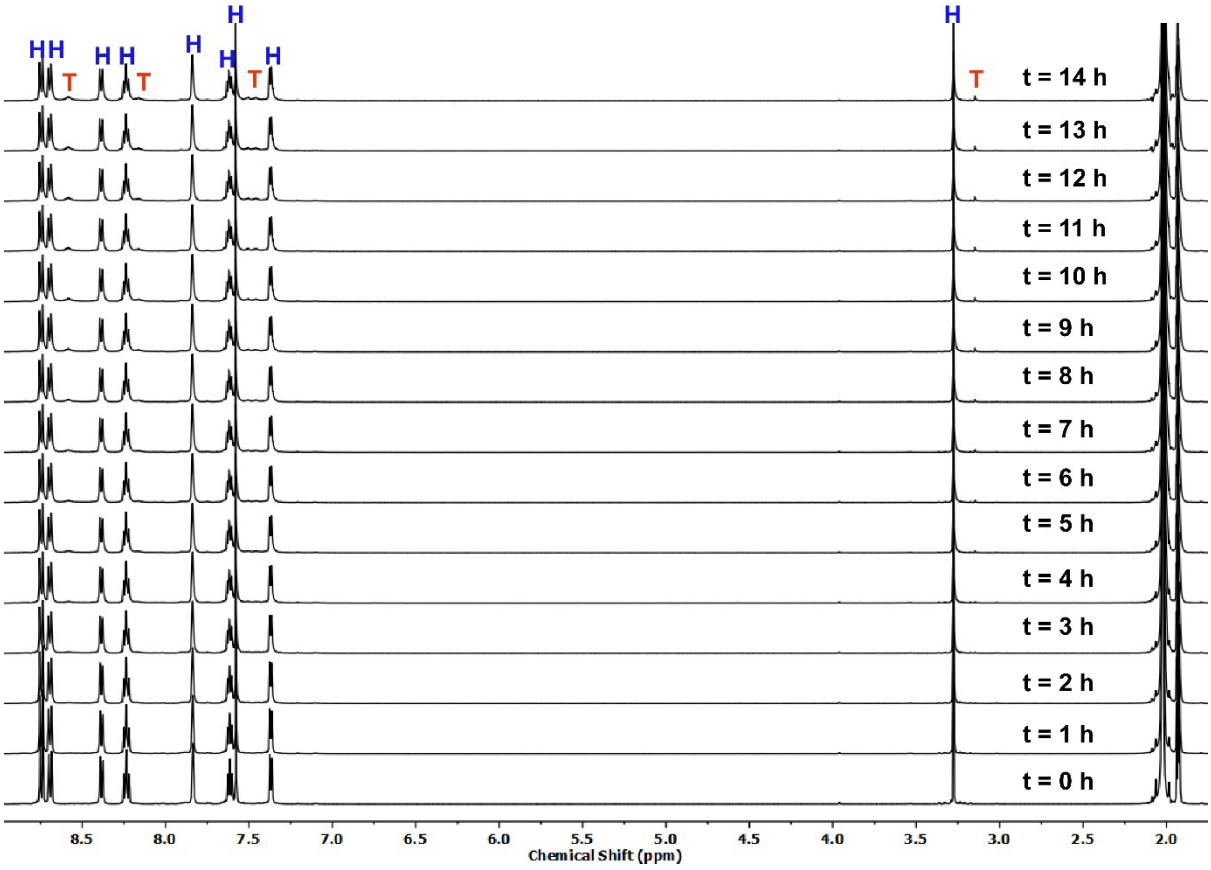

Figure S31. Representative ^{1}H NMR spectra (500 MHz, CD_3CN) showing the growth of the tetrahedral assembly from helical assembly as function of time at 343 K.

1.3.4 In situ ^{1}H NMR study of half concentration of $[Fe_2\mathbf{L}_3]^{8+}$ at 343 K

7.5 mg of $[Fe_2\mathbf{L}_3]^{4+}$ (half concentration of **H**) was dissolved in 0.8 mL CD_3CN and the ^{1}H NMR was recorded at 10-minute intervals at 343 K over 16 hrs *in-situ* in the NMR A set of spectra is depicted in Figure S32.

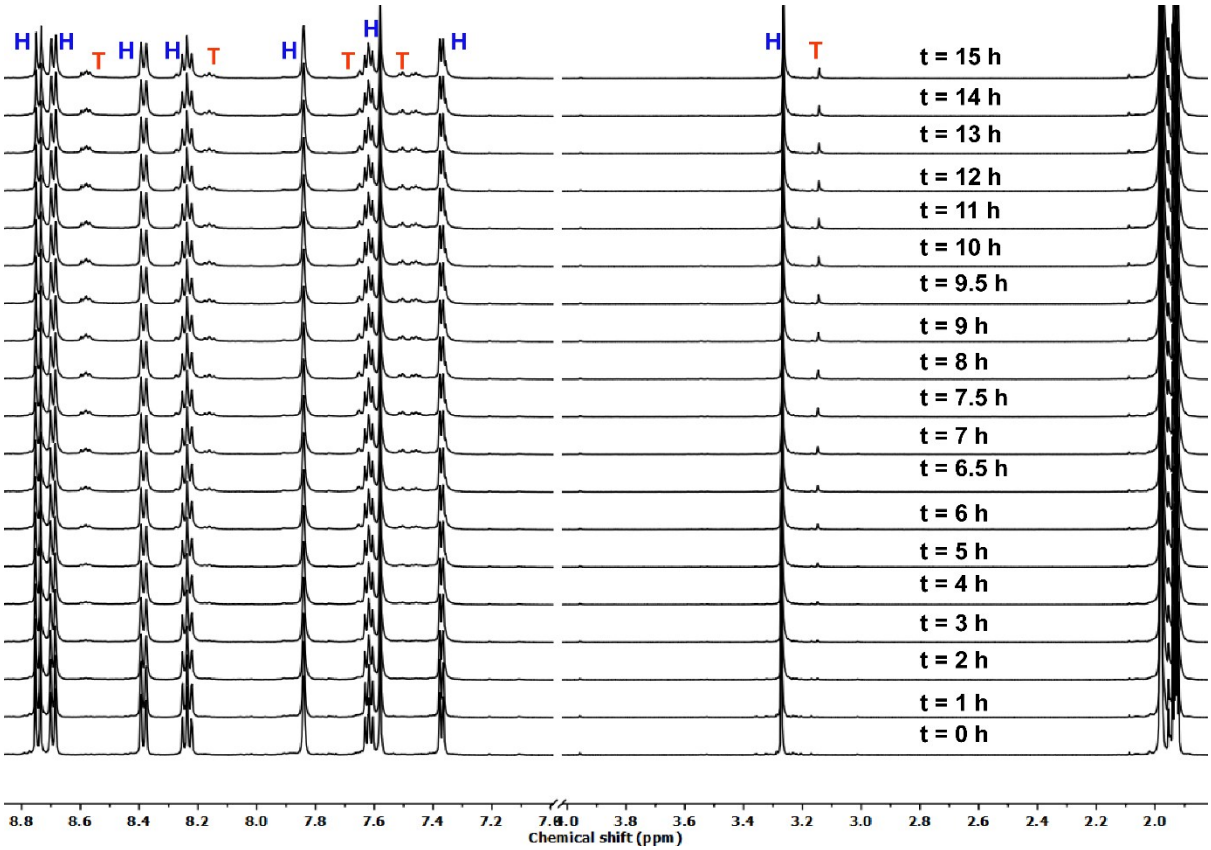

Figure S32. Selected ^{1}H NMR spectra (500 MHz, CD_3CN) showing the growth of the tetrahedron assembly from helical assembly as function of time at 343K.

1.3.5 In situ ^{1}H NMR study of $[Fe_2\mathbf{L}_3]^{8+}$ at 253 K

3 mg of $[Fe_2\mathbf{L}_3]^{4+}$ (**H**) was dissolved in 0.6 mL CD_3CN and the ^{1}H NMR was recorded at 10-minute intervals at 253 K over 18 hrs *in-situ*. A set of spectra is depicted in Figure S33.

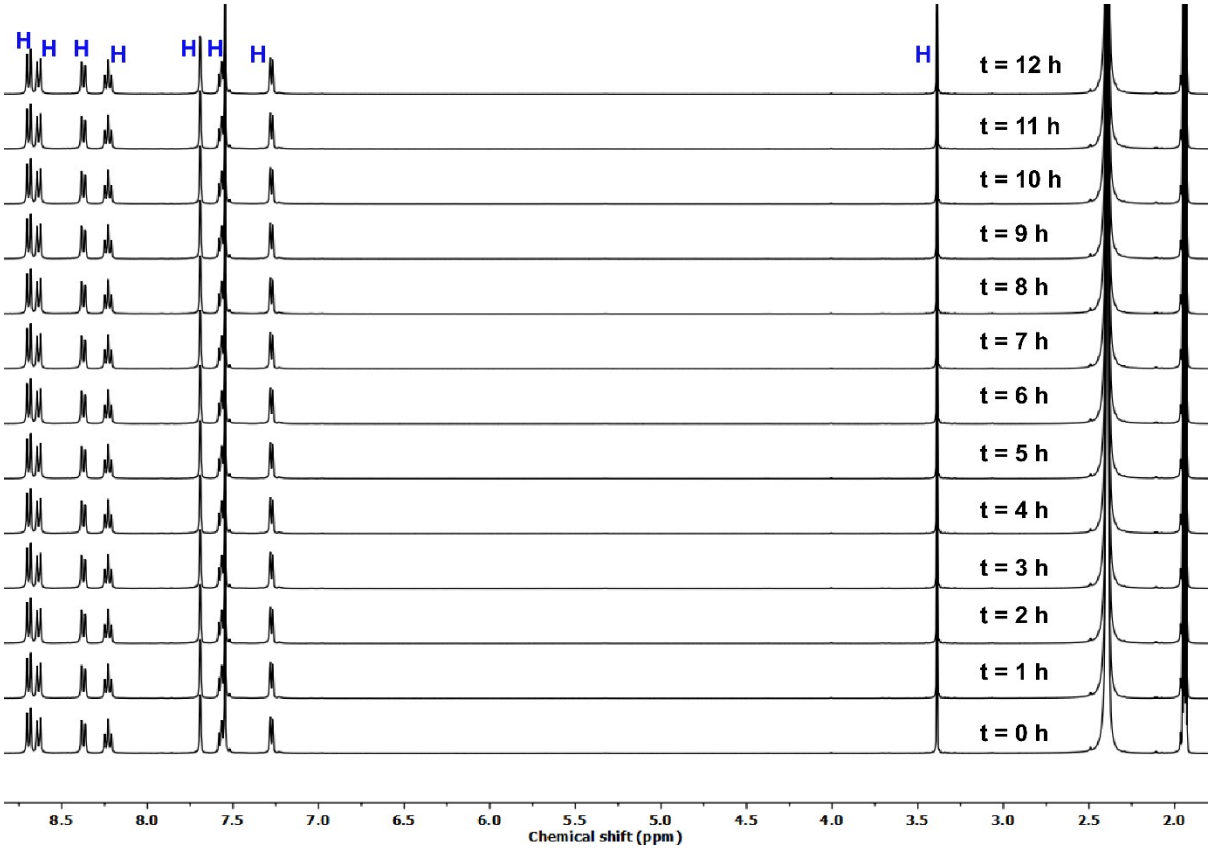

Figure S33. Selected ^{1}H NMR spectra (400 MHz, CD_3CN) showing there is no growth of the tetrahedron assembly from helical assembly at lower temperature 253 K.

1.3.6 Guest binding study of equilibrated $[Fe_2\mathbf{L}_3]^{8+}$ and $[Fe_4\mathbf{L}_6]^{8+}$

An NMR tube was charged with equilibrated 0.8 mL of the PF_6 salt mixture of $[Fe_2\mathbf{L}_3]^{8+}$ and $[Fe_4\mathbf{L}_6]^{8+}$ and 2 eq of sodium tetrafluoroborate was added. After closing the NMR tube, the reaction mixture was shaken for 30 s and then stored at 298 K ~1 h for equilibration. Then ^{19}F NMR spectra was recorded as below. There were no appreciable shifts from the expected unencapsulated fluorine peak positions nor appearance of additional peaks indicative of anion encapsulation for either the BF_4^- or PF_6^-. This suggests no anion encapsulation occurred in either the tetrahedron or the helicate. ^{19}F NMR (470 MHz, CD_3CN) δ -72.72 (d, J = 707.0 Hz), -151.51 (s).

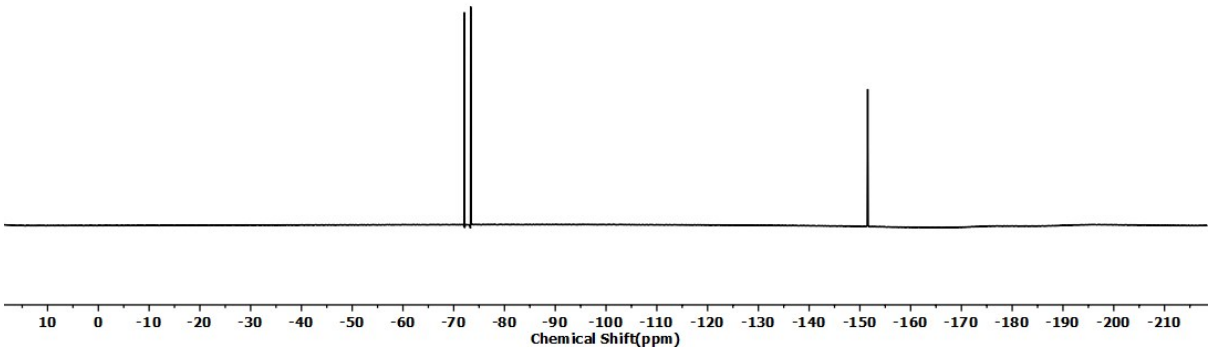

Figure S34. ^{19}F NMR spectrum (470 MHz, CD_3CN) showing there was no guest encapsulated in the cage.

1.4 Scrambling experiments

*1.4.1 In situ ^{1}H NMR scrambling study of $[Fe_4L_6]^{4+}$ (**T**) and $[Fe_4L'_6]^{4+}$ (**Q**) at 343K*

3 mg of $[Fe_4L_6]^{8+}$ (**T**) and 3 mg of $[Fe_4L'_6]^{4+}$ (**Q**) was dissolved in 0.6 mL CD_3CN and the ^{1}H NMR was recorded at 10-minute at 343 K over 24 hrs *in-situ* in the NMR. A set of spectra is depicted in Figure S35.

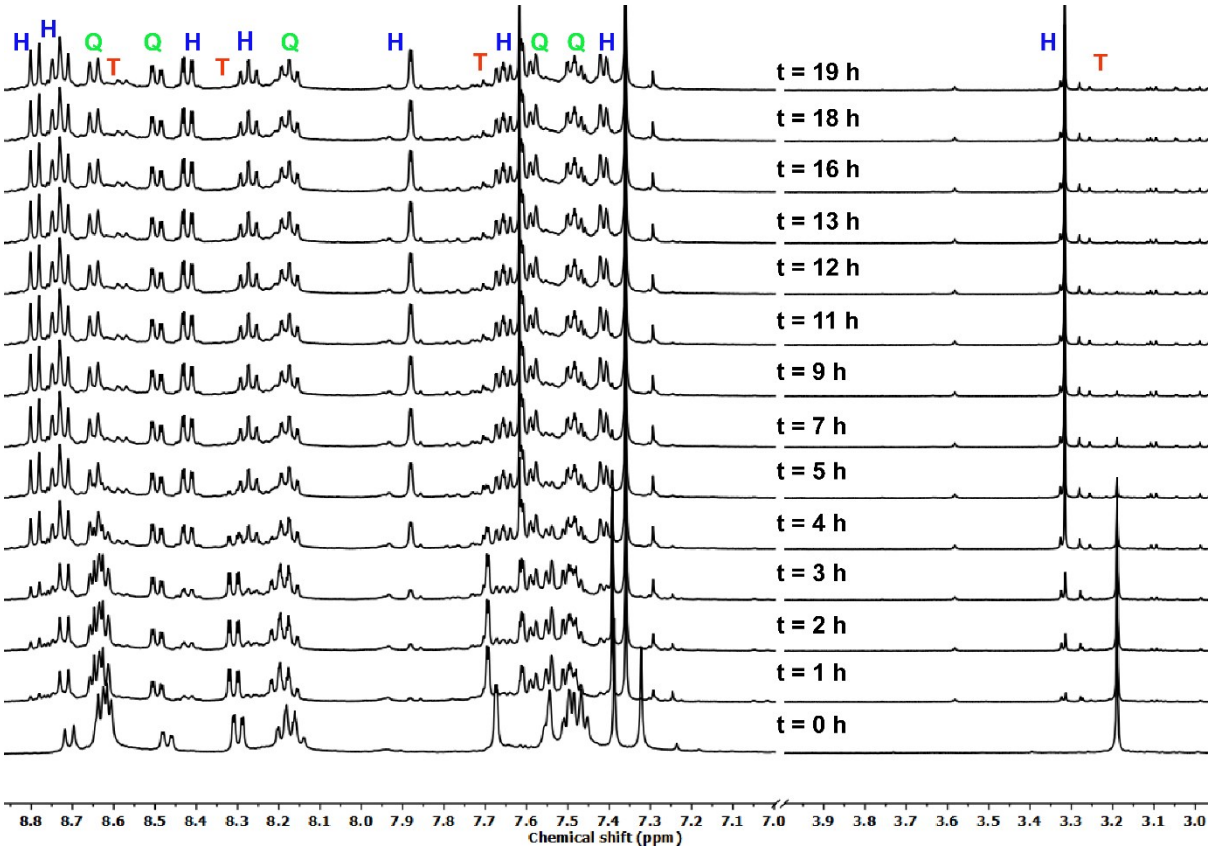

Figure S35. Selected ^{1}H NMR spectra (400 MHz, CD_3CN) showing the growth of the helical assembly (**H**) from tetrahedron assembly (**T**) but no change $[Fe_4L'_6]^{4+}$ (**Q**) as function of time at 343K.

1.5 Determination of rate constants

1.5.1 Development of a kinetic model

We postulate that the interconversion of helicate (H) -tetrahedron (T) interconversion passes through an intermediate (X) and thus this is a three-state system (1).

$$2H \rightleftharpoons 2X \rightleftharpoons T \qquad (1)$$

As outlined in the procedure of Helfferich, each step of this reaction is statistically independent, coupled only through the mutual dependence of shared participants.[12] Each micro-step of the mechanism can be described by the following rates.

For $2H \rightleftharpoons 2X$ which is a unimolecular process, with the forward and reverse rate constants k_1^H and k_{-1}^H, the rate at which H is consumed is defined by

$$r_H = -k_1^H[H] \qquad (2a)$$

and the rate at which X appears is

$$r_X = +k_1^H[H] \qquad (2b)$$

For the reverse process the rate at which X disappears is

$$r_X = -k_{-1}^H[X] \qquad (2c)$$

and the rate at which H appears is

$$r_H = +k_{-1}^H[X] \qquad (2d)$$

For the conversion of X to T, which is a bimolecular process with the forward and reverse rate constants k_2^H and k_{-2}^H, the rate at which X disappears is

$$r_X = -2k_2^H[X]^2 \qquad (2e)$$

and the rate at which T appears is

$$r_T = +k_2^H[X]^2 \qquad (2f)$$

and thus $r_X = -2\, r_T$

The conversion of T to X, which is a unimolecular process, the rate at which T disappears is

$$r_T = -k_{-2}^H[T] \qquad (2g)$$

and the rate at which X appears is

$$r_X = +k_{-2}^H[T] \qquad (2h)$$

Combining terms gives three rate equations for the conversion of H to T

$$\frac{dH}{dt} = -k_1^H[H] + k_{-1}^H[X] \qquad (3a)$$

$$\frac{dX}{dt} = +k_1^H[H] - k_{-1}^H[X] - 2k_2^H[X]^2 + k_{-2}^H[T] \qquad (3b)$$

$$\frac{dT}{dt} = +k_2^H[X]^2 - k_{-2}^H[T] \qquad (3c)$$

This is an example of a "non-simple" kinetic pathway because the intermediate can react with itself[12] and no analytical solutions to these three differential equations exist although numerical methods can be used (see Section 1.5.5 below).

It is, however, also possible to approximate (1) as a two state system (4)

$$2H \rightleftharpoons T \qquad (4)$$

with the apparent rate constants k_f^H (for the forward reaction) and k_r^H (for the reverse reaction) such that

$$k_f^H = \frac{k_1^H k_2^H}{k_{-1}^H + k_2^H} \qquad (5)$$

and

$$k_r^H = \frac{k_{-1}^H k_{-2}^H}{k_{-1}^H + k_2^H} \qquad (6)$$

so that

$$K_{eq} = \frac{k_f^H}{k_r^H} = \frac{\dfrac{k_1^H k_2^H}{k_{-1}^H + k_2^H}}{\dfrac{k_{-1}^H k_{-2}^H}{k_{-1}^H + k_2^H}} = \frac{k_1^H k_2^H}{k_{-1}^H k_{-2}^H}$$

the use of the apparent rate constants does allow an analytical solution as follows.

1.5.2 Derivation of reversible 2:1 integrated rate law using the apparent rate constants

Consider the equilibrium between 2[M_2L_3] (H) and [M_4L_6] (T)

$$2H \rightleftharpoons T \qquad (7)$$

The equilibrium constant K is given by (8). As this is a reversible reaction define the rate constants for the forward reaction k_f and the reverse reaction k_r.

$$K = \frac{[T]}{[H]^2} = \frac{k_f}{k_r} \qquad (8)$$

The units for k_f are $M^{-1}s^{-1}$ and for k_r are s^{-1}.

The rate of the reaction is defined as

$$\text{Rate} = -\frac{1}{2}\frac{d[H]}{dt} = \frac{d[T]}{dt} \qquad (8a)$$

The rate laws for this reversible reaction is given by

$$\frac{-1}{2}\frac{d[H]}{dt} = k_f[H]^\alpha - k_r[T]^\beta \qquad (9)$$

and

$$-\frac{d[T]}{dt} = k_r[T]^\beta - k_f[H]^\alpha \qquad (9a)$$

for a first order reaction in each direction $\alpha = \beta = 1$ giving

$$\frac{-1d[H]}{2dt} = k_f[H] - k_r[T] \qquad (10)$$

if only [H] is present at time = 0 then from (7)

$$[T]_t = \frac{1}{2}([H]_0 - [H]_t) \qquad (11)$$

and if only [T] is present at time = 0 then from (7)

$$[H]_t = 2([T]_0 - [T]_t) \qquad (12)$$

and at equilibrium

$$K = \frac{\frac{1}{2}([H]_0 - [H]_{eq})}{[H]_{eq}{}^2} = \frac{k_f}{k_r} \qquad (13)$$

which can be solved for $[H]_0$

$$[H]_0 = \frac{[H]_{eq}(2k_f[H]_{eq} + k_r)}{k_r} \qquad (14)$$

Substituting (11) into (10) gives

$$\frac{-1d[H]}{2dt} = k_f[H] - k_r\frac{1}{2}([H]_0 - [H]) = \quad (k_f + \frac{1}{2}k_r)[H] - \frac{1}{2}k_r[H]_0 \qquad (15)$$

and (14) into (15)

$$\frac{-d[H]}{dt} = \quad (2k_f + k_r)[H] - [H]_{eq}(2k_f[H]_{eq} + k_r) \qquad (16)$$

Which can be integrated as follows

$$-\int_{[H]_0}^{[H]_t} \frac{d[H]}{(2k_f + k_r)[H] - [H]_{eq}(2k_f[H]_{eq} + k_r)} = \int_0^t dt \qquad (17)$$

$$-\left[\frac{ln\{\ (2k_f + k_r)[H] - [H]_{eq}(2k_f[H]_{eq} + k_r)\ \}}{2k_f + k_r}\right]_0^t = t \qquad (18)$$

$$-\left[\frac{ln\{\ (2k_f + k_r)[H]_t - [H]_{eq}(2k_f[H]_{eq} + k_r)\}}{2k_f + k_r} - \frac{ln\{\ (2k_f + k_r)[H]_0 - [H]_{eq}(2k_f[H]_{eq} + k_r)\}}{2k_f + k_r}\right] = t \quad (19)$$

$$-ln\left[\frac{(2k_f + k_r)[H]_t - [H]_{eq}(2k_f[H]_{eq} + k_r)}{(2k_f + k_r)[H]_0 - [H]_{eq}(2k_f[H]_{eq} + k_r)}\right] = (2k_f + k_r)t \quad (20)$$

$$ln\left[\frac{(2k_f + k_r)[H]_0 - [H]_{eq}(2k_f[H]_{eq} + k_r)}{(2k_f + k_r)[H]_t - [H]_{eq}(2k_f[H]_{eq} + k_r)}\right] = (2k_f + k_r)t \quad (21)$$

Which can be rearranged to

$$\frac{(2k_f + k_r)[H]_0 - [H]_{eq}(2k_f[H]_{eq} + k_r)}{(2k_f + k_r)[H]_t - [H]_{eq}(2k_f[H]_{eq} + k_r)} = e^{(2k_f + k_r)t} \quad (22)$$

$$\frac{(2k_f [H]_{eq}{}^2 - 2k_f[H]_0 + k_r([H]_{eq} - [H]_0))}{([H]_t(-2k_f - k_r) + 2k_f[H]_{eq}{}^2 + k_r[H]_{eq})} = e^{(2k_f + k_r)t} \quad (23)$$

and substituting using the solution to following solution to the quadratic form of (13)

$$0 = [H]_{eq}{}^2 + \frac{1}{2}\frac{k_r}{k_f}[H]_{eq} - \frac{1}{2}\frac{k_r}{k_f}[H]_0$$

$$[H]_{eq} = -\frac{1}{4}\left(\frac{k_r}{k_f} - \sqrt{\frac{k_r}{k_f}\left(\frac{k_r}{k_f} + 8[H]_0\right)}\right) \quad (24)$$

$$\frac{2k_f[H]_0}{2k_f[H]_t + k_r([H]_t - [H]_0)} = e^{(2k_f + k_r)t} \quad (25)$$

And

$$\frac{2k_f[H]_0 e^{-(2k_f + k_r)t} + k_r[H]_0}{2k_f + k_r} = [H]_t \quad (26)$$

and using (11)

$$[H]_t + 2[T]_t = [H]_0$$

$$[T]_t = \frac{1}{2}[H]_0 - \frac{2k_f[H]_0 e^{-(2k_f + k_r)t} + k_r[H]_0}{2(2k_f + k_r)} \quad (27)$$

both (5) and (6) can then substituted into (26) and (27).

1.5.3 Derivation of reversible 1:2 integrated rate law using the apparent rate constants

consider

$$T \rightleftharpoons 2H \qquad (28)$$

The equilibrium constant K is given by (29). As this is a reversible reaction defines the rate constants for the forward reaction k_f and the reverse reaction k_r.

$$K = \frac{[H]^2}{[T]} = \frac{k_f}{k_r} \qquad (29)$$

The units for k_f are s^{-1} and for k_r are $M^{-1}s^{-1}$.

The rate of the reaction is defined as

$$\text{Rate} = +\frac{1}{2}\frac{d[H]}{dt} = -\frac{d[T]}{dt} \qquad (30)$$

The rate laws for this reversible reaction is given by

$$-\frac{d[T]}{dt} = k_f[T]^{\alpha} - k_r[H]^{\beta} \qquad (31)$$

and

$$-\frac{1}{2}\frac{d[H]}{dt} = k_r[H]^{\beta} - k_f[T]^{\alpha} \qquad (32)$$

for a first order reaction in each direction $\alpha = \beta = 1$ giving

$$\frac{-d[T]}{dt} = k_f[T] - k_r[H] \qquad (33)$$

if only [T] is present at time = 0 then from (28)

$$[T]_t = [T]_0 - 1/2[H]_t \qquad (34)$$

and if only [H] is present at time = 0 then from (28)

$$[H]_t = [H]_0 - 2[T]_t \qquad (35)$$

Putting (34) into (29)

$$K = \frac{(2([T]_0 - [T]_{eq}))^2}{[T]_{eq}} = \frac{k_f}{k_r} \qquad (36)$$

Which can be solved to give

$$[T]_0 = [T]_{eq} \pm \frac{\sqrt{k_f}\sqrt{[T]_{eq}}}{2\sqrt{k_r}} \quad (37)$$

of which only

$$[T]_0 = [T]_{eq} + \frac{\sqrt{k_f}\sqrt{[T]_{eq}}}{2\sqrt{k_r}} \quad (38)$$

is physically meaningful as $[T]_0 > [T]_{eq}$

Substituting (34) into (33) gives

$$\frac{-d[T]}{dt} = k_f[T] - 2k_r([T]_0 - [T]) = k_f[T] - 2k_r[T]_0 + 2k_r[T] = [T](k_f + 2k_r) - 2k_r[T]_0 \quad (39)$$

And (38) into (39)

$$\frac{-d[T]}{dt} = [T](k_f + 2k_r) - 2k_r\left([T]_{eq} + \frac{\sqrt{k_f}\sqrt{[T]_{eq}}}{2\sqrt{k_r}}\right) \quad (40)$$

Integrating (40)

$$\int_{[T]_0}^{[T]_t} \frac{-d[T]}{[T](k_f + 2k_r) - 2k_r\left([T]_{eq} + \frac{\sqrt{k_f}\sqrt{[T]_{eq}}}{2\sqrt{k_r}}\right)} = \int_0^t dt \quad (41)$$

$$-\left[\frac{ln\left\{\sqrt{k_f}\sqrt{k_r}\sqrt{[T]_{eq}} + 2k_r[T]_{eq} - k_f[T] - 2k_r[T])\right\}}{(k_f + 2k_r)}\right]_0^t = t \quad (42)$$

$$-ln\frac{\left\{(k_f + 2k_r)[T]_t - 2k_r[T]_{eq} - \sqrt{k_f}\sqrt{k_r}\sqrt{[T]_{eq}}\right\}}{\left\{(k_f + 2k_r)[T]_0 - 2k_r[T]_{eq} - \sqrt{k_f}\sqrt{k_r}\sqrt{[T]_{eq}}\right\}} = (k_f + 2k_r)t \quad (43)$$

$$\frac{\left\{(k_f + 2k_r)[T]_0 - 2k_r[T]_{eq} - \sqrt{k_f}\sqrt{k_r}\sqrt{[T]_{eq}}\right\}}{\left\{(k_f + 2k_r)[T]_t - 2k_r[T]_{eq} - \sqrt{k_f}\sqrt{k_r}\sqrt{[T]_{eq}}\right\}} = e^{(k_f + 2k_r)t} \quad (44)$$

$$\frac{\left\{(k_f + 2k_r)[T]_0 - 2k_r[T]_{eq} - \sqrt{k_f}\sqrt{k_r}\sqrt{[T]_{eq}}\right\}e^{-(k_f + 2k_r)t} + \sqrt{k_f}\sqrt{k_r}\sqrt{[T]_{eq}} + 2k_r[T]_{eq}}{(k_f + 2k_r))} = [T]_t$$

(45)

using (34)

$$[H]_t = 2[T]_0 - \frac{2\left\{(k_f + 2k_r)[T]_0 - 2k_r[T]_{eq} - \sqrt{k_f}\sqrt{k_r}\sqrt{[T]_{eq}}\right\}e^{-((k_f + 2k_r)t} + \sqrt{k_f}\sqrt{k_r}\sqrt{[T]_{eq}} + 2k_r[T]_{eq}}{(k_f + 2k_r))}$$

(46)

from (36)

$$\frac{(2([T]_0 - [T]_{eq}))^2}{[T]_{eq}} = \frac{k_f}{k_r}$$

$$[T]_{eq} = \frac{k_f + 8k_r[T]_0 \pm \sqrt{k_f}\sqrt{k_f + 16k_r[T]_0}}{8k_r} \qquad (47)$$

Of which only

$[T]_{eq} = \frac{k_f + 8k_r[T]_0 - \sqrt{k_f}\sqrt{k_f + 16k_r[T]_0}}{8k_r}$ is physically meaningful as To must be > than Teq. (48)

$$\frac{\left\{(k_f + 2k_r)[T]_0 - \frac{k_f + 8k_r[T]_0 - \sqrt{k_f}\sqrt{k_f + 16k_r[T]_0}}{4} - \sqrt{k_f}\sqrt{k_r}\sqrt{\frac{k_f + 8k_r[T]_0 - \sqrt{k_f}\sqrt{k_f + 16k_r[T]_0}}{8k_r}}\right\}e^{-(k_f + 2k_r)t} + \sqrt{k_f}\sqrt{k_r}\sqrt{\frac{k_f + 8k_r[T]_0 - \sqrt{k_f}\sqrt{k_f + 16k_r}}{8k_r}}}{(k_f + 2k_r))} = [T]_t \quad (49)$$

and

$$2[T]_0 - \frac{2\left\{(k_f + 2k_r)[T]_0 - \frac{k_f + 8k_r[T]_0 - \sqrt{k_f}\sqrt{k_f + 16k_r[T]_0}}{4} - \sqrt{k_f}\sqrt{k_r}\sqrt{\frac{k_f + 8k_r[T]_0 - \sqrt{k_f}\sqrt{k_f + 16k_r[T]_0}}{8k_r}}\right\}e^{-(k_f + 2k_r)t} + \sqrt{k_f}\sqrt{k_r}\sqrt{\frac{k_f + 8k_r[T]_0 - \sqrt{k_f}\sqrt{k_f + 1}}{8k_r}}}{(k_f + 2k_r))} = [H]_t \quad (50)$$

Both (5) and (6) can then be substituted into (49) and (50)

1.5.4 Data fitting using the derived rate laws to obtain the apparent rate constants.

The concentration isotherms of the interconversion (*section 1.3.2, 1.3.3 and 1.3.4)* of the helicates and the tetrahedra as a function of time were fitted with the derived rate laws (*section 1.5.2* and *1.5.3*) with the computer programme *Prism 8*[13]. The resulting fits and associated statistics for the conversion of the tetrahedron into the helicate are given in figures S36 and S37, and those for the conversion of the helicate to the tetrahedron are given in figures S38, S39, S40 and S41.

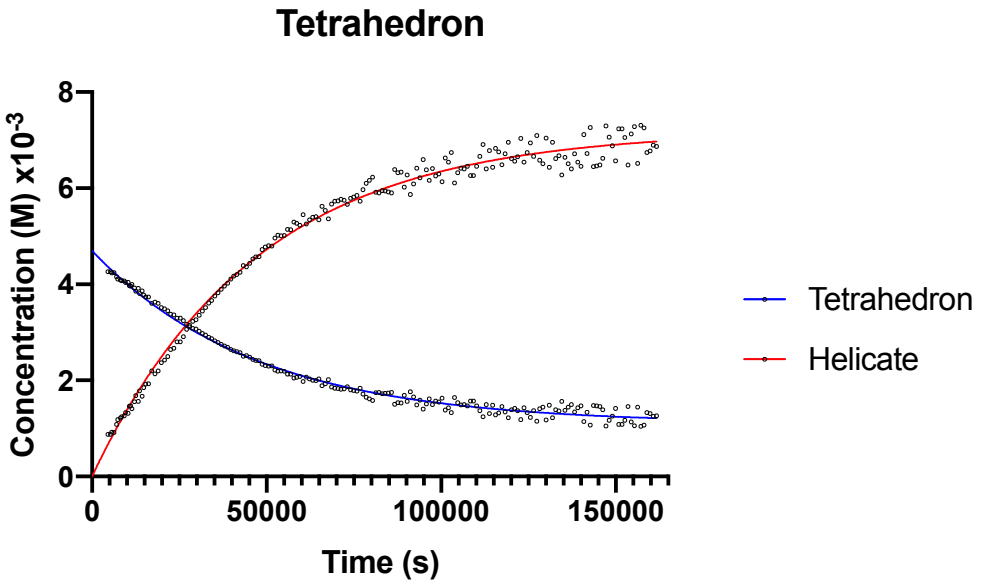

Figure S36. Plot of relative concentrations of **T** ($[Fe_4\mathbf{L}_6]^{8+}$) and **H** ($[Fe_2\mathbf{L}_3]^{4+}$) as function of time, when pure tetrahedral assembly was the starting point.

	Nonlin fit Table of results	A	B	C
		Tetrahedron (mM)	Helicate (mM)	Global (shared)
		Y	Y	Y
1	**First order reversible 1:2 combined all**			
2	**Best-fit values**			
3	kf	1.637e-005	1.637e-005	1.637e-005
4	kr	2.500e-006	2.500e-006	2.500e-006
5	To	= 4.700	= 4.700	
6	**95% CI (profile likelihood)**			
7	kf	1.613e-005 to 1.661e-005	1.613e-005 to 1.661e-005	1.613e-005 to 1.661e-005
8	kr	2.394e-006 to 2.607e-006	2.394e-006 to 2.607e-006	2.394e-006 to 2.607e-006
9	**Goodness of Fit**			
10	Degrees of Freedom			364
11	R squared	0.9899	0.9899	0.9950
12	Sum of Squares	1.621	6.483	8.103
13	Sy.x			0.1492
14	**Constraints**			
15	kf	kf is shared	kf is shared	
16	kr	kr is shared	kr is shared	
17	To	To = 4.7	To = 4.7	
18				
19	**Number of points**			
20	# of X values	183	183	

Figure S37. The resulting fits and associated statistics for the conversion of the tetrahedron into the helicate.

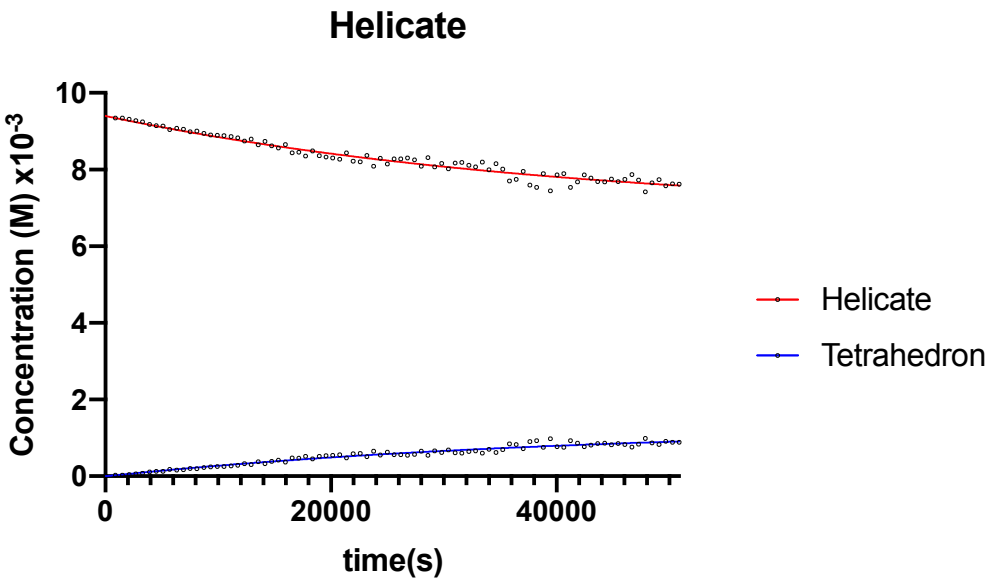

Figure S38. Plot of relative concentrations of **T** and **H** as function of time, when pure helical assembly was the starting point.

	Nonlin fit Table of results	A Helicate (mM)	B Tetrahedron (mM)	C Global (shared)
		Y	Y	Y
1	**First order reversible 2:1 combined**			
2	**Best-fit values**			
3	Ho	= 9.400	= 9.400	
4	kf	3.291e-006	3.291e-006	3.291e-006
5	kr	1.743e-005	1.743e-005	1.743e-005
6	**95% CI (profile likelihood)**			
7	kf	3.112e-006 to 3.479e-006	3.112e-006 to 3.479e-006	3.112e-006 to 3.479e-006
8	kr	1.431e-005 to 2.065e-005	1.431e-005 to 2.065e-005	1.431e-005 to 2.065e-005
9	**Goodness of Fit**			
10	Degrees of Freedom			166
11	R squared	0.9540	0.9540	0.9995
12	Sum of Squares	1.081	0.2703	1.352
13	Sy.x			0.09023
14	**Constraints**			
15	Ho	Ho = 9.4	Ho = 9.4	
16	kf	kf is shared	kf is shared	
17	kr	kr is shared	kr is shared	
18				
19	**Number of points**			
20	# of X values	84	84	

Figure S39. The resulting fits and associated statistics for the conversion of the helicate into the tetrahedron.

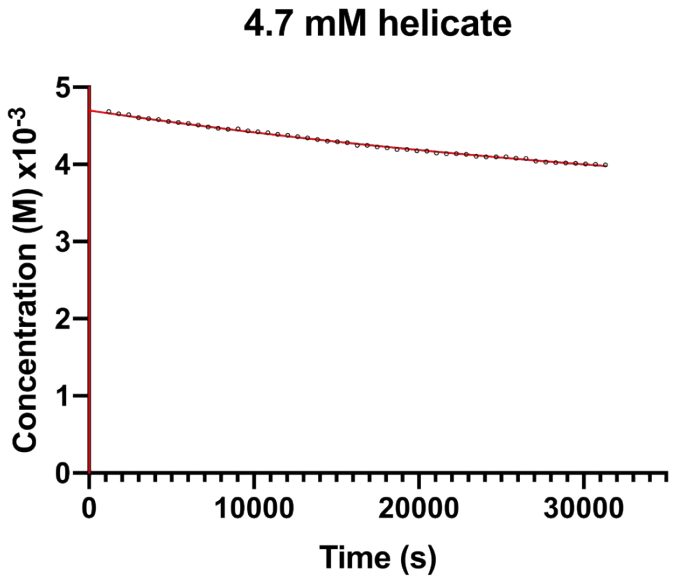

Figure S40. Plot of relative concentrations of **H** as function of time, when pure helical assembly was the starting point at half the concentration..

Nonlin fit Table of results		A Helicate (mM)
		Y
1	**First order reversible 2:1**	
2	**Best-fit values**	
3	Ho	= 4.700
4	kf	3.353e-006
5	kr	1.459e-005
6	**95% CI (profile likelihood)**	
7	kf	3.266e-006 to 3.442e-006
8	kr	1.235e-005 to 1.687e-005
9	**Goodness of Fit**	
10	Degrees of Freedom	49
11	R squared	0.9972
12	Sum of Squares	0.006019
13	Sy.x	0.01108
14	**Constraints**	
15	Ho	Ho = 4.7
16		
17	**Number of points**	
18	# of X values	51
19	# Y values analyzed	51

Figure S41. The resulting fits and associated statistics for the conversion of the helicate into the tetrahedron.

1.5.5 Application of numerical methods to find solutions for 3a-3c.

The following *Mathematica* program was written to find the solutions to differential equations for 3a-c, i.e. the time-dependence of the concentrations of *H(t)* and *T(t)* and perform a non-linear least squares fit to obtain the four rate constants using the same isotherms as above (*section 1.3.2* and *1.3.3)*.

```
Remove["Global`*"];

em[name_String, size_ : 2] := Graphics[{Dynamic@ EdgeForm@Directive[CurrentValue["Color"],(*JoinForm["Round"],*)
    AbsoluteThickness[2], Opacity[1]], FaceForm[White], ResourceFunction["PolygonMarker"][name, Offset[size]]}]

MyRed = RGBColor[0.7961, 0.3922, 0.3804];  MyYellow = RGBColor[0.8706, 0.7725, 0.4196];
MyGreen = RGBColor[0.3373, 0.5804, 0.5098];  MyBlue = RGBColor[0.3216, 0.4078, 0.6432];

HTdat = Import["/path/HT.csv", "Data"];
   lHT = Length[HTdat];
   HTdatH = Table[{HTdat[[i, 1]], HTdat[[i, 2]]}, {i, 2, lHT}];
   HTdatT = Table[{HTdat[[i, 1]], HTdat[[i, 3]]}, {i, 2, lHT}];
   MatrixForm[HTdatH];  MatrixForm[HTdatT];

THdat = Import["/path/T2H.csv", "Data"];
   lTH = Length[THdat];
   THdatT = Table[{THdat[[i, 1]], THdat[[i, 2]]}, {i, 2, lTH}];
   THdatH = Table[{THdat[[i, 1]], THdat[[i, 3]]}, {i, 2, lTH}];
   MatrixForm[THdatT]; MatrixForm[THdatH];

plHTH = ListPlot[HTdatH, PlotStyle -> MyRed, PlotRange -> {{-100, 200000}, {-1, 10}}, PlotMarkers -> em /@ {"Circle"},
   IntervalMarkers -> "Fences", IntervalMarkersStyle -> Directive[MyRed, Thick], ImageSize -> 20/2.54*72, Frame -> True,
   FrameStyle -> Thick, FrameLabel -> {"Time (s)", "Concentration (mM)"}, RotateLabel -> True, LabelStyle -> {Black, FontWeight
   -> Plain, FontSize -> 18}];
plHTT = ListPlot[HTdatT, PlotStyle -> MyBlue, PlotRange -> {{-100, 200000}, {-1, 10}}, PlotMarkers -> em /@ {"Diamond"},
   IntervalMarkers -> "Fences", IntervalMarkersStyle -> Directive[MyBlue, Thick], ImageSize -> 20/2.54*72, Frame -> True,
   FrameStyle -> Thick, FrameLabel -> {"Time (s)", "Concentration (mM)"}, RotateLabel -> True, LabelStyle -> {Black, FontWeight
   .-> Plain, FontSize -> 18}];
plTHT = ListPlot[THdatT, PlotStyle -> Orange, PlotRange -> {{-100, 200000}, {-1, 10}}, PlotMarkers -> em /@ {"Square"},
   IntervalMarkers -> "Fences", IntervalMarkersStyle -> Directive[MyRed, Thick], ImageSize -> 20/2.54*72, Frame -> True,
   FrameStyle -> Thick, FrameLabel -> {"Time (s)", "Concentration (mM)"}, RotateLabel -> True, LabelStyle -> {Black, FontWeight
   -> Plain, FontSize -> 18}];
plTHH = ListPlot[THdatH, PlotStyle -> MyGreen, PlotRange -> {{-100, 200000}, {-1, 10}}, PlotMarkers -> em /@ {"Triangle"},
   IntervalMarkers -> "Fences", IntervalMarkersStyle -> Directive[MyBlue, Thick], ImageSize -> 20/2.54*72, Frame -> True,
   FrameStyle -> Thick, FrameLabel -> {"Time (s)", "Concentration (mM)"}, RotateLabel -> True, LabelStyle -> {Black, FontWeight
   -> Plain, FontSize -> 18}];
pldata = Show[plHTH, plHTT, plTHT, plTHH]; (*Export["data.pdf",%]*)

data = Join[{1, Sequence @@ #} & /@ HTdatH, {2, Sequence @@ #} & /@ HTdatT, {3, Sequence @@ #} & /@ THdatT, {4, Sequence
   @@ #} & /@  THdatH]; MatrixForm[data];

ndsol2 = ParametricNDSolveValue[{
   HTH'[t] == -kHX HTH[t] + kXH HTX[t],
   HTX'[t] == +kHX HTH[t] - kXH HTX[t] - 2 kXT HTX[t]^2 + 2 kTX HTT[t],
   HTT'[t] ==                                  +   kXT HTX[t]^2  -     kTX HTT[t],
   HTH[0] == 9.4,
   HTX[0] == 0,
   HTT[0] == 0,
   THT'[t] == -   kTX THT[t]   + kXT THX[t]^2,
   THX'[t] == +2 kTX THT[t] - 2 kXT THX[t]^2 - kXH THX[t] + kHX THH[t],
   THH'[t] ==                                      + kXH THX[t]   - kHX THH[t],
   THT[0] == 4.7,
   THX[0] == 0,
   THH[0] == 0},
   {HTH, HTX, HTT, THH, THX, THT}, {t, 0, 200000}, {kHX, kXH, kXT, kTX}, StepMonitor :> Print["monitoring ks ", {kHX, kXH, kXT,
      kTX}]]

lpstatic = Plot[Evaluate[#[t] & /@ ndsol2[0.000012, 0.000624, 0.004950, 0.000077]], {t, 0, 200000}, PlotStyle -> {MyRed, Brown,
   MyBlue, MyGreen, Purple, Orange}, PlotLegends -> {HTH, HTX, HTT, THH, THX, THT}, PlotRange -> {{0, 200000}, {0, 10}}];
Show[pldata, lpstatic];  Export["chi.by.eye.fit.pdf", %];
```

```
model[kHX_, kXH_, kXT_, kTX_][j_, t_] := Through[ndsol2[kHX, kXH, kXT, kTX][t], List][[j]] /; And @@ NumericQ /@ {kHX, kXH, kXT,
    kTX, j, t};

fit = NonlinearModelFit[data, model[kHX, kXH, kXT, kTX][j, t], {{kHX, 0.000012}, {kXH, 0.000624}, {kXT, 0.004950}, {kTX,
    0.000077}}, {j, t}]
fit["RSquared"];  fit["ParameterTable"];  MatrixForm[fit["CorrelationMatrix"]];

plfit = Plot[{fit[1, t], fit[2, t], fit[3, t], fit[4, t], fit[5, t], fit[6, t]}, {t, 0, 200000}, PlotStyle -> {MyRed, Brown, MyBlue, MyGreen, Purple,
    Orange}];
plall = Show[pldata, plfit];  Export["best.fit.pdf", %]
```

Setting $k_1^H = 0.000012$ s^{-1}, $k_{-1}^H = 0.000624$ s^{-1}, $k_2^H = 0.004950$ mM^{-1} s^{-1}, and $k_{-2}^H = 0.000077$ s^{-1} gave the following fit (Figure S42):

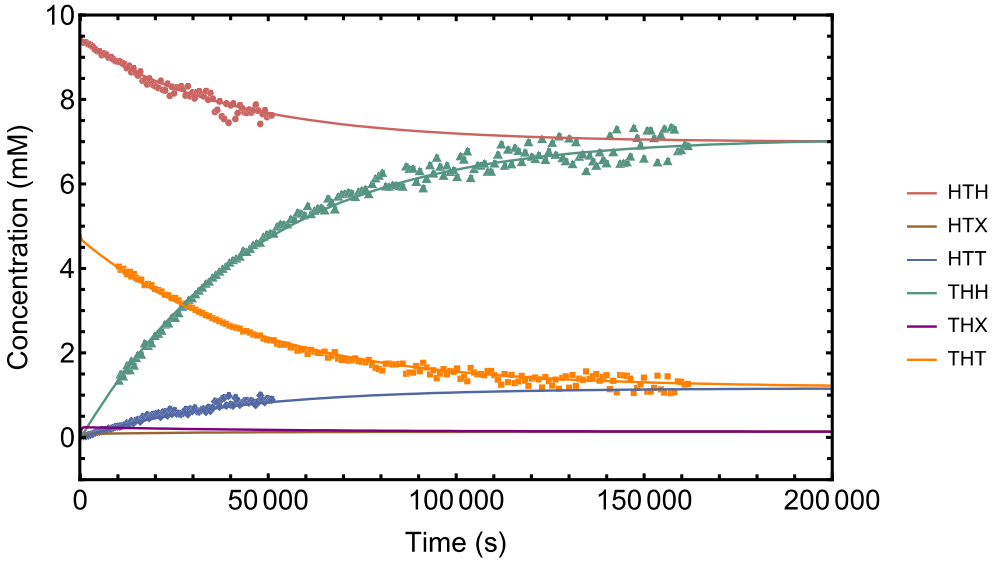

Figure S42. The resulting fits and associated statistics for the numerical integration of the helicate into the tetrahedron and conversion of tetrahedron to helicate.

Although these initial values give a very good visual fit, an actual least squares fit did not converge because of covariance between two of the fitted parameters k_2^H and k_{-1}^H (as the intermediate was not observed). Nevertheless, the modelling does provide an estimate of the individual rate constants which could then be used with the analytical solutions.

1.5.6 Data fitting using the derived rate laws to estimate the individual rate constants.

The concentration isotherms of the interconversion (*section 1.3.2 and 1.3.3)* of the helicates and the tetrahedra as a function of time were then again fitted with the derived rate laws (*section 1.5.1* and *1.5.2*) using the substitutions of (5) and (6) with the computer programme *Prism 8*[13] and a global fit. The covariant parameters k_2^H and k_{-1}^H were fixed to the values obtained by the numerical methods ie $k_{-1}^H =$ 0.000624 s^{-1} and k_2^H 0.004950 mM^{-1} s^{-1} . The resulting fits and associated statistics for the conversion of the tetrahedron into the helicate are given in Figures S43 and S44, and those for the conversion of the helicate to the tetrahedron are given in Figures S45 and S46. In order to comply with the syntax requirements of the software k_{-1}^H was denoted k_3 and k_{-2}^H was denoted k_4.

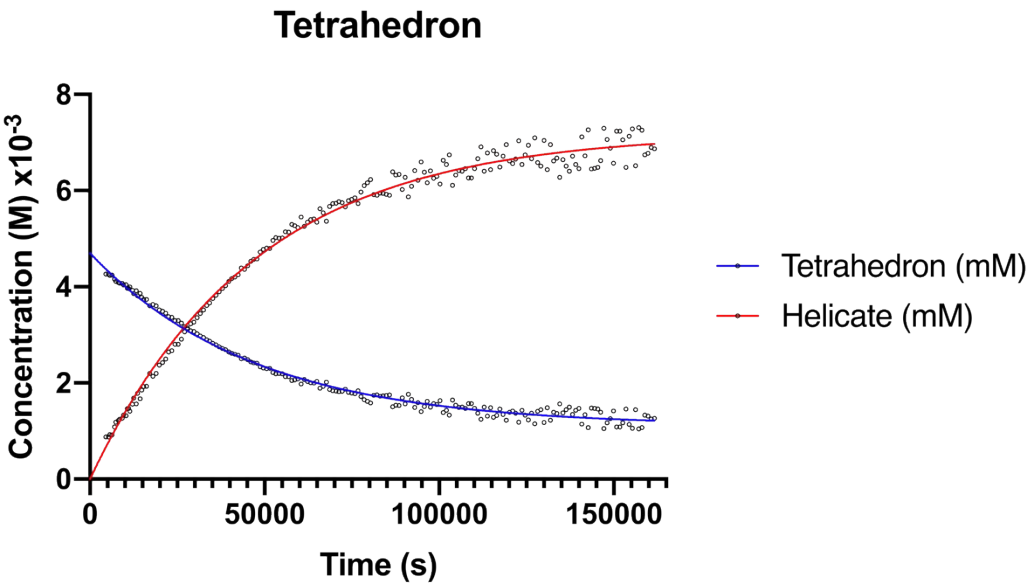

Figure S42. Plot of relative concentrations of **T** ($[Fe_4\mathbf{L}_6]^{8+}$) and **H** ($[Fe_2\mathbf{L}_3]^{4+}$) as function of time, when pure tetrahedral assembly was the starting point.

	Nonlin fit Table of results	A	B	C
		Tetrahedron (mM)	Helicate (mM)	Global (shared)
		Y	Y	Y
1	**First order reversible 1:2 combined all test**			
2	**Best-fit values**			
3	To	= 4.700	= 4.700	
4	k1	0.0001462	0.0001462	0.0001462
5	k2	= 0.0006240	= 0.0006240	
6	k3	= 0.004950	= 0.004950	
7	k4	2.815e-006	2.815e-006	2.815e-006
8	**95% CI (profile likelihood)**			
9	k1	0.0001441 to 0.0001484	0.0001441 to 0.0001484	0.0001441 to 0.0001484
10	k4	2.696e-006 to 2.936e-006	2.696e-006 to 2.936e-006	2.696e-006 to 2.936e-006
11	**Goodness of Fit**			
12	Degrees of Freedom			364
13	R squared	0.9899	0.9899	0.9950
14	Sum of Squares	1.621	6.483	8.103
15	Sy.x			0.1492
16	**Constraints**			
17	To	To = 4.7	To = 4.7	
18	k1	k1 is shared	k1 is shared	
19	k2	k2 = 0.000624	k2 = 0.000624	
20	k3	k3 = 0.00495	k3 = 0.00495	
21	k4	k4 is shared	k4 is shared	
22				
23	**Number of points**			
24	# of X values	183	183	
25	# Y values analyzed	183	183	

Figure S43. The resulting fits and associated statistics for the conversion of the tetrahedron into the helicate.

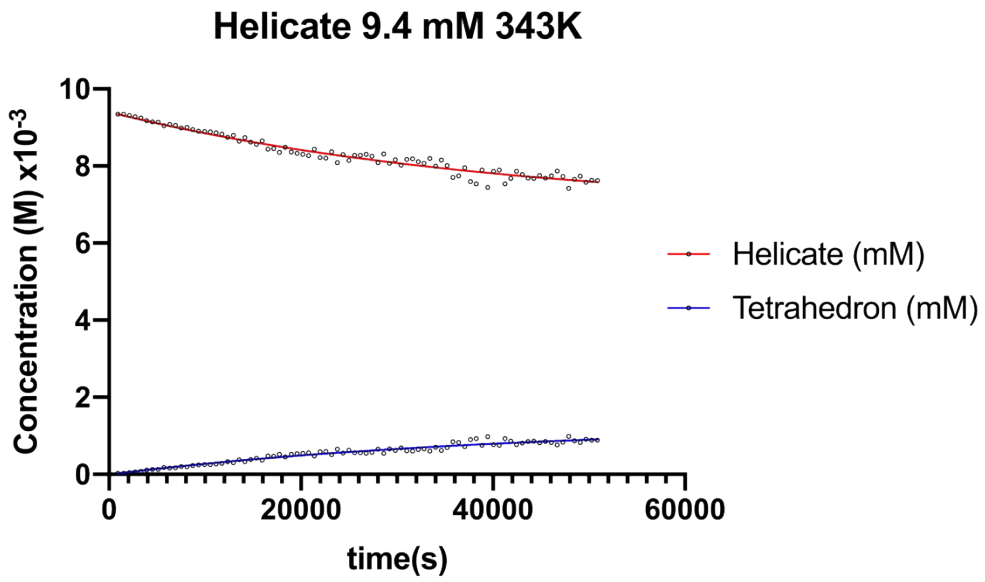

Figure S44. Plot of relative concentrations of **T** and **H** as function of time, when pure helical assembly was the starting point.

Nonlin fit Table of results		A	B	C
		Helicate (mM)	Tetrahedron (mM)	Global (shared)
		Y	Y	Y
1	**First order reversible 2:1 combined test**			
2	**Best-fit values**			
3	Ho	= 9.400	= 9.400	
4	k1	3.705e-006	3.705e-006	3.705e-006
5	k2	= 0.004950	= 0.004950	
6	k3	= 0.0006240	= 0.0006240	
7	k4	0.0001557	0.0001557	0.0001557
8	**95% CI (profile likelihood)**			
9	k1	3.504e-006 to 3.917e-006	3.504e-006 to 3.917e-006	3.504e-006 to 3.917e-006
10	k4	0.0001278 to 0.0001845	0.0001278 to 0.0001845	0.0001278 to 0.0001845
11	**Goodness of Fit**			
12	Degrees of Freedom			166
13	R squared	0.9540	0.9540	0.9995
14	Sum of Squares	1.081	0.2703	1.352
15	Sy.x			0.09023
16	**Constraints**			
17	Ho	Ho = 9.4	Ho = 9.4	
18	k1	k1 is shared	k1 is shared	
19	k2	k2 = 0.00495	k2 = 0.00495	
20	k3	k3 = 0.000624	k3 = 0.000624	
21	k4	k4 is shared	k4 is shared	
22				
23	**Number of points**			
24	# of X values	84	84	
25	# Y values analyzed	84	84	

Figure S45. The resulting fits and associated statistics for the conversion of the helicate into the tetrahedron.

1.6 References

1. Coulson, D. R.; Satek, L. C.; Grim, S. O., Tetrakis(triphenylphosphine)palladium(0). *Inorg. Synth.* **2007**, 121-124.
2. Norio, M.; Akira, S., Palladium-Catalyzed Reaction of 1-Alkenylboronates with Vinylic Halides: (1z,3e)-1-Phenyl-1,3-Octadiene. *Organic Syntheses* **1990,** *68*, 130.
3. Pefkianakis, E. K.; Tzanetos, N. P.; Kallitsis, J. K., Synthesis and Characterization of a Novel Vinyl-2,2′-bipyridine Monomer and Its Homopolymeric/Copolymeric Metal Complexes. *Chem. Mater.* **2008,** *20* (19), 6254-6262.
4. He, F.; Wang, W.; Chen, W.; Xu, T.; Darling, S. B.; Strzalka, J.; Liu, Y.; Yu, L., Tetrathienoanthracene-Based Copolymers for Efficient Solar Cells. *J. Am. Chem. Soc.* **2011,** *133* (10), 3284-3287.
5. Duhović, S.; Dincă, M., Synthesis and Electrical Properties of Covalent Organic Frameworks with Heavy Chalcogens. *Chem. Mater.* **2015,** *27* (16), 5487-5490.
6. Burke, M. J.; Nichol, G. S.; Lusby, P. J., Orthogonal Selection and Fixing of Coordination Self-Assembly Pathways for Robust Metallo-organic Ensemble Construction. *J. Am. Chem. Soc.* **2016,** *138* (29), 9308-9315.
7. Cowieson, N. P.; Aragao, D.; Clift, M.; Ericsson, D. J.; Gee, C.; Harrop, S. J.; Mudie, N.; Panjikar, S.; Price, J. R.; Riboldi-Tunnicliffe, A.; Williamson, R.; Caradoc-Davies, T., MX1: a bending-magnet crystallography beamline serving both chemical and macromolecular crystallography communities at the Australian Synchrotron. *J. Synch. Rad.* **2015,** *22* (1), 187-190.
8. Kabsch, W., XDS. *Acta Cryst.* **2010,** *D66*, 125-32.
9. Sheldrick, G., SHELXT - Integrated space-group and crystal-structure determination. *Acta Cryst.* **2015,** *71* (1), 3-8.
10. Dolomanov, O. V.; Bourhis, L. J.; Gildea, R. J.; Howard, J. A. K.; Puschmann, H., OLEX2: a complete structure solution, refinement and analysis program. *J. Appl. Cryst.* **2009,** *42* (2), 339-341.
11. Sheldrick, G., A short history of SHELX. *Acta Cryst.* **2008,** *64* (1), 112-122.
12. Helfferich, F. G., Kinetics of Multistep Reactions. In *In Comprehensive Chemical Kinetics*, Green, N. J. B., Ed. Elsevier: 2004; Vol. 40.
13. Ivashchenko, R. *Prism 8 for macOS*, 8.4.3; GraphPad Software, LLC: 2020.